Impact of mixing state and hygroscopicity on CCN activity of biomass burning aerosol in Amazonia

Madeleine Sánchez Gácita[1], Karla M. Longo[1,a], Julliana L. M. Freire[1], Saulo R. Freitas[1,a], Scot T. Martin[2]

5   [1] Center for Weather Forecasting and Climate Research, INPE, Cachoeira Paulista, SP, Brazil
[2] School of Engineering and Applied Science, Harvard University, Cambridge, MA, USA
[a] Now at Universities Space Research Association/Goddard Earth Sciences Technology and Research (USRA/GESTAR) at Global Modeling and Assimilation Office, NASA Goddard Space Flight Center, Greenbelt, MD, USA

Correspondence to: M. Sánchez Gácita (madeleine.sanchez@cptec.inpe.br)

10   **Abstract.** Smoke aerosols prevail throughout Amazonia because of widespread biomass burning during the dry season, and external mixing, low variability in the particle size distribution and low particle hygroscopicity are typical. There can be profound effects on cloud properties. This study uses an adiabatic cloud model to simulate the activation of smoke particles as cloud condensation nuclei (CCN) for three hypothetical case studies, chosen as to resemble biomass burning aerosol observations in Amazonia. The relative importance of variability in hygroscopicity, mixing state, and activation kinetics for

15   the activated fraction and maximum supersaturation are assessed. For a population with $\kappa_p = 0.04$, an overestimation of the cloud droplet number concentration N_d for the three selected case studies between 22.4 ± 1.4 % and 54.3 ± 3.7 % was obtained when assuming an hygroscopicity parameter $\kappa_p = 0.20$. Assuming internal mixing of the aerosol population lead to overestimations of up to 20% of N_d when a group of particles with medium hygroscopicity was present in the externally mixed population cases. However, the overestimations were below 10% for external mixtures between very low and low

20   hygroscopicity particles, as seems to be the case for Amazon smoke particles. Kinetic limitations were significant for medium and high hygroscopicity, and much lower very low and low hygroscopicity particles. When particles were assumed to be at equilibrium and to respond instantly to changes in the air parcel supersaturation, the overestimation of the droplet concentration was up to ~100% in internally mixed populations, and up to ~250% in externally mixed ones, being larger for the higher values of hygroscopicity. In addition, a perceptible delay between the times when maximum supersaturation and

25   maximum aerosol activated fraction are reached was noticed and, for aerosol populations with effective hygroscopicity $\kappa_{p_{eff}}$ higher than a certain threshold value, the delay in particle activation was such that no particles were activated at the time of maximum supersaturation. Considering internally mixed populations, for an updraft velocity $W = 0.5$ m s^{-1} this threshold of no activation varied between $\kappa_{p_{eff}} = 0.35$ and $\kappa_{p_{eff}} = 0.5$ for the different case studies. However, for low hygroscopicity kinetic limitations played a weaker role for CCN activation of particles, even when taking into account the large aerosol

30   mass and number concentrations. For the very low range of hygroscopicities, the overestimation of the droplet concentration

due to the equilibrium assumption was lowest and the delay between the times when maximum supersaturation and maximum activated fraction were reached was greatly reduced or no longer observed (depending on the case study). These findings on uncertainties and sensitivities provide guidance on appropriate simplifications that can be used for modeling of smoke aerosols within general circulation models. The use of medium values of hygroscopicity representative of smoke aerosols for other biomass burning regions on Earth can lead to significant errors, compared to the use of low hygroscopicity for Amazonia (between 0.05 and 0.13, according to available observations). Also in this region, to consider the biomass burning population as internally mixed will lead to small errors in the droplet concentration, while significantly increasing the computational burden. Regardless of the large smoke aerosol loads in the region during the dry season, kinetic limitations are expected to be low.

1 Introduction

Aerosol-cloud interactions are a major source of uncertainties in the quantification of climate forcing of aerosols (Bauer and Menon, 2012; IPCC, 2013). The wet size of an aerosol particle when at equilibrium with the environment is governed by Köhler theory (Köhler, 1936) and depends on particle size and composition. In the atmosphere, activation of cloud condensation nuclei (CCN) is a competition between aerosol particles for water vapor, influenced by dynamical processes and the kinetics of particle growth and dependent on the updraft velocities, aerosol number concentrations and differences in size and composition of aerosol particles (McFiggans et al., 2006). Although our understanding of the processes involved in aerosol activation has increased considerably in recent years (Farmer et al., 2015), the inclusion of all the detailed information that might be available about aerosol populations into global and regional circulation models is often impractical. Thus, assessments of the uncertainties derived from simplifications assumed are relevant and potentially contribute to the discussion on the level of sophistication required by general circulation models (GCMs) with the aim of decreasing the uncertainties.

A large quantity of aerosol particles is generated globally by open biomass burning (Granier et al., 2011; Lamarque et al., 2010; van der Werf et al., 2010), and the impacts of smoke aerosols in climate, air quality and geochemistry have being addressed in several studies (Andreae, 1991; Crutzen and Andreae, 1990; Jacobson, 2004; Langmann et al., 2009; Tosca et al., 2013, and references there in). Vegetation fires plumes can be entrained into upper levels of the troposphere and undergo long-range transport before being removed from the atmosphere if conditions are favorable, e.g. when convection activity is high, (Andreae, 1991; Andreae et al., 2001; Freitas et al., 2005; Fromm and Servranckx, 2003). During the dry season in South America, observation and numerical model results agree in that biomass burning aerosol originated from extensive fires typically detected over the Amazon and Central Brazil regions, represents a significant fraction of the aerosol burden in South and Southeast parts of Brazil, Uruguay and the Northern of Argentina (Camponogara et al., 2014; Freitas et al., 2005; Longo et al., 2010; Ramanathan, 2001; Rosário et al., 2013; Wu et al., 2011).

Even though a large fraction of biomass burning aerosols has low to moderate hygroscopicity (Carrico et al., 2010; Dusek et al., 2011; Engelhart et al., 2012; Petters et al., 2009; Rissler et al., 2006), biomass burning particles can act as CCN under sufficiently high atmospheric water vapor supersaturations (Mircea et al., 2005; Rose et al., 2010; Vestin et al., 2007). Therefore, CCN activation properties of pyrogenic particles are likely to be relevant for the aerosol climate forcing.

Some external mixing in terms of hygroscopicity seems to be rather common in aerosol populations, particularly over continents (Kandler and Schütz, 2007; Swietlicki et al., 2008). Yet, average hygroscopicity parameters have been estimated from both observational and modeled data assuming internal mixing for aerosols from the same emission source (e.g., biomass burning), or even within the same geographical region (Gunthe et al., 2009; Pringle et al., 2010). Sensitivity of CCN activation to hygroscopic mixing state under equilibrium conditions is also significant, and the assumption of total internal mixing could result in an overestimation of the CCN population that can range from 10% to 100% (Cubison et al., 2008; Ervens et al., 2010; Padró et al., 2012; Wex et al., 2010). The impact of mixing state under dynamic conditions has, however, been less studied, and some evidence suggests that conclusions from equilibrium conditions might not be directly extrapolated to CCN activation during cloud formation (Cubison et al., 2008; Ervens et al., 2010).

The aerosol particle's composition is known to influence the particle water uptake and CCN activation (Almeida et al., 2014; Mircea et al., 2005; Roberts et al., 2003). Although the effects of composition on the cloud droplet number concentrations are typically secondary when compared to those of population number concentration and size distribution (Dusek et al., 2006; Feingold, 2003; Hudson, 2007; McFiggans et al., 2006; Reutter et al., 2009), the extent to which its complexities can be safely neglected in GCMs is also yet to be established. Droplet number concentrations were shown to be more sensitive to the presence of organic content than to the updraft velocity in some situations (Rissman et al., 2004). On conditions typical of pyrocumulus (number concentrations up to 10^5 cm^{-3} and updraft velocities up to 20 m s^{-1}), Reutter et al. (2009) found that cloud droplet number concentration was sensitive to compositional effects (hygroscopicity). For three different ratios of the aerosol number concentrations to the updraft velocity, and for a fixed aerosol size distribution, the authors found that the sensitivity to hygroscopicity was low for medium to high hygroscopic values, but moderate for very low and low hygroscopicity values (Reutter et al., 2009). Still, sensitivities to hygroscopicity are likely to be tightly related to the position of the dry critical size of the smallest activated particle within the overall size distribution of the aerosol population, and significant sensitivities have been obtained for the population of small aerosol particles with medium and high hygroscopicity (Ward et al., 2010).

Aerosol particles with critical supersaturations smaller than the maximum supersaturation reached within the cloud can nonetheless become interstitial aerosols due to the evaporation and deactivation mechanisms described by Nenes et al. (2001). These kinetic limitations, sometimes neglected in GCMs, are expected to be large when significant aerosol loads are present (Nenes et al., 2001). Consequently, parameterizations that assume equilibrium conditions overestimate CCN when kinetic limitations are important (Nenes et al., 2001; Phinney et al., 2003). However, little is known about how kinetic limitations are related with the particle hygroscopicity, although a relation between the timescale of the components solubility and activation has been reported (Chuang, 2006).

On the other hand, several observational biomass burning studies conducted in the Amazon region reported rather similar number size distributions for biomass burning aerosols within the boundary layer (Andreae et al., 2004; Artaxo et al., 2013; Brito et al., 2014; Reid et al., 1998; Rissler et al., 2004, 2006). In terms of hygroscopicity, these smoke particles have been found to be externally mixed (Rissler et al., 2004, 2006). Their population effective hygroscopicity parameter, converted from the original data using expressions suggested by Gunthe et al. (2009), ranged between 0.05 and 0.13 (Rissler et al., 2004, 2006), and compare well with observed values for biomass burning aerosols, but are rather on the lower side of the range of values reported elsewhere. Reported values of the hygroscopicity parameter for freshly emitted smoke particles in biomass burning laboratory experiments reached values up to 0.6, although a significant amount of data indicated values between 0.02 and 0.2, with wood species and smoldering fires producing the less hygroscopic particles (Carrico et al., 2010; Dusek et al., 2011; Engelhart et al., 2012; Petters et al., 2009). An average hygroscopicity parameter of 0.21 was obtained for a four days biomass burning episode near Guangzhou, China using airborne data (Rose et al., 2010). The hygroscopicity parameter obtained from CCN airborne measurements for boreal fires biomass burning aerosols in Canada was 0.18 for both recently emitted and aged aerosols, while the values estimated assuming an average chemical composition were, on average, 0.11 for fresh aerosol particles and 0.24 for aged ones, both within the level of variability of the value estimated from CCN measurements (Lathem et al., 2013). A recent study of the hygroscopicity of recently emitted and aged smoke particles reported ranging between 0.05-0.1 for the same parameter in Thailand (Hsiao et al., 2016).

In the present study, we used an adiabatic cloud model to simulate the CCN activation of biomass burning particles, aiming to contribute to the understanding of the possible impact of different hygroscopicity values, mixing state and kinetic limitations in the CCN activated fraction. The modeling approach followed is described in Sect. 2. According to the available observations of biomass burning aerosols in the Amazon region, three typical situations in terms of size distributions and other aerosol parameters were considered in the definition of the case studies and other simulation parameters, as described in Sect. 3. Finally, the results from the cloud parcel model and our conclusions are discussed in Sect. 4 and Sect. 5.

2 Modeling approach

2.1 Cloud parcel model

A model of an air parcel assumed to ascend adiabatically at a prescribed updraft velocity and without entrainment to supersaturation conditions was used to study the activation of aerosol particles in the first stages of cloud development. The air parcel model used in this work is based on the model described by Pruppacher and Klett (Pruppacher and Klett, 1997), with the supersaturation and liquid water mixing ratio tendencies estimated as in Seinfeld and Pandis (2006) and the equilibrium supersaturation calculated as proposed by Petter and Kreidenweiss using the hygroscopicity parameter κ_P (2007). The pressure is estimated assuming the environment is in hydrostatic equilibrium, and the temperature and water

vapor mixing ratio are estimated from the moisture and heat conservation, respectively (Pruppacher and Klett, 1997). The surface tension dependence on temperature is relevant to CCN activation (Christensen and Petters, 2012), and it is calculated as $\sigma_{w/a} = 7.61 \times 10^{-2} - 1.55 \times 10^{-4}(T - 273.15)$ (Seinfeld and Pandis, 2006).

The aerosol dry size distribution for each hygroscopic group is discretized into n bins with a fixed volume ratio for all bins.
5   Particles that belong to bin size i and hygroscopic group h are assumed to grow equally when exposed to the same conditions. Coagulation and coalescence processes are not considered, so the number of particles in each bin remains constant while their wet sizes change over time (full-moving size structure) (Jacobson, 2005). In this work, the particle's critical diameter is determined for each bin size and hygroscopic group as the value that maximized the particle's equilibrium supersaturation. Aerosol particles with wet size larger than their critical size are considered activated. Particles
10   larger than strictly activated particles are considered cloud droplets as well because they have wet sizes larger than that of cloud droplets and can condense significant quantities of water vapor on their surfaces (Nenes et al., 2001). The total cloud droplet number concentration estimated without assuming equilibrium conditions, $N_{d,neq}$, is the sum of strictly activated particles and those with wet sizes larger than activated particles. To abbreviate the notation, hereafter N_d will refer to $N_{d,neq}$ at the end of the simulation, unless otherwise stated.
15   Some parameterizations of CCN activation neglect kinetic limitations (Ghan et al., 2011). A notable example of one of such parameterizations is the one proposed by Abdul-Razzak and Ghan (Abdul-Razzak and Ghan, 2000, 2002), widely used in GCMs (Ban-weiss et al., 2014; Bauer et al., 2010; He et al., 2015; Makkonen et al., 2014; Pierce et al., 2015 and references therein). In this parameterization is assumed that particles are in equilibrium with the environment until the maximum supersaturation is reached and consider as activated all particles with critical supersaturation less or equal to the air parcel
20   maximum supersaturation. If particles are presumed to respond instantly to changes in the air parcel supersaturation, particles with critical supersaturation lower than a given supersaturation s will also have dry sizes larger than a dry particle cut diameter $d_{dry,c}$ (details in Appendix B). The cloud droplet concentration estimated thus, here denoted $N_{d,eq}$, effectively represent the maximum cloud droplet concentration attainable at supersaturation s. If evaporation and deactivation mechanisms of kinetic limitations (Nenes et al., 2001) are significant, the calculation of the cloud droplet spectra from the
25   maximum supersaturation assuming equilibrium will lead to an overestimation of the cloud droplet number concentration. In an intermediate approach, particles can be considered cloud droplets if their wet diameters are larger than the approximate cut wet diameter d_c that corresponds to $d_{dry,c}$ in equilibrium conditions (Appendix B). This approximate estimation, denoted N_{d,neq_simp}, considers kinetic effects to some extent since the wet sizes of particles that are compared to d_c are calculated explicitly in the cloud model. In order to measure the impact of kinetic limitations in the simulations, estimations by the
30   three aforementioned methods are presented. In addition, the ratio between the equilibrium droplet concentration

corresponding to the maximum supersaturation and the droplet concentration, $\max(N_{d,eq})/N_{d,neq}$, was estimated at the time of maximum supersaturation and at the end of the simulation.

The cloud parcel model described was fully implemented in *Mathematica*® 10.0 (Wolfram Research, 2014). Equations for the size of particles in each bin, supersaturation, liquid water mixing ratio, water vapor mixing ratio, air pressure and temperature form a closed system of $n+5$ non-linear ordinary differential equations (ODE) in which derivatives depend not only on the set of variables but on their derivatives as well. The ODE system was solved using IDA method from SUNDIAL package (SUite of Nonlinear and DIfferential/ALgebraic equation Solvers) (Hindmarsh, 2000; Hindmarsh and Taylor, 1999), as implemented in the function NDSOLVE of *Mathematica*.

2.6 Sensitivity of CCN to a parameter

Sensitivities $S(X_i)$ in the context of CCN activation were first introduced by Feingold (2003) as the slope in the linear regression to the logarithms of cloud-top effective droplet radius r_{eff} as a function of the logarithms of the parameter X_i, i.e. $S_{X_i} = \partial \ln r_{eff} / \partial \ln X_i$. Later on, McFiggans et al. (2006) proposed sensitivities of the droplet number concentration N_d to a parameter X_i:

$$S_{X_i} = \frac{\partial \ln(N_d)}{\partial \ln(X_i)} \tag{7}$$

According to Eq. (7), $N_d \propto X_i^{S_{X_i}}$, and a sensitivity closer to zero indicate a smaller increase in N_d as parameter X_i increases. Sensitivities were calculated from linear regressions in $\ln(N_d)$ vs. $\ln(X_i)$ curves as averages (slope of the linear fit) and locally (derivatives of the curves in the $\ln - \ln$ space).

3 Definition of case studies and simulation parameters

In this work, three hypothetical different size distributions were defined as case studies for the cloud model simulations (Table 1). The corresponding number size distributions are depicted in Fig. 1. The parameters of the selected size distributions were chosen as to resemble biomass burning aerosol observations in Amazonia (resumed in Table S1 of the Supplement) while trying to minimize the impact of particle size and standard deviation. First, a moderately polluted case with 5000 cm^{-3} particles in the Aitken mode, and 1000 cm^{-3} in the accumulation modes, respectively (MP$_{5,1}$) (Fig. 1, a). Case MP$_{5,1}$ is similar to the observed distribution during the SAMBBA experiment (South American Biomass Burning Analysis, 2012) (Brito et al., 2014). Second, a case study with the same number concentration than MP$_{5,1}$, but with higher number of particles in the accumulation mode, with 1000 cm^{-3} and 5000 cm^{-3} in the accumulation and Aitken modes, respectively (MP$_{1,5}$) (Fig. 1, b). The size distribution of case MP$_{1,5}$ is comparable to the observed during LBA-SMOCC (Large-Scale Biosphere Atmosphere Experiment in Amazonia - Smoke Aerosols, Clouds, Rainfall, and Climate, 2002) dry-to-wet

transition period. There was also a predominance of particles in the accumulation mode during the biomass burning episodes of LBA-CLAIRE (Cooperative LBA Airborne Regional Experiment, 2001) (Rissler et al., 2004), although particle number concentrations were lower for these periods. Finally, a highly polluted case (HP$_{5,5}$) (Fig. 1, c) with 5000 cm^{-3} in both modes, resembling the observed distribution during the SMOCC dry period (Rissler et al., 2006), minus the nucleation mode.

5   Particles in the nucleation mode are not expected to impact significantly the CCN behavior of the aerosol population and were disregarded.

In both CLAIRE and SMOCC experiments, smoke particles were found to be externally mixed in terms of hygroscopicity (Rissler et al., 2004, 2006). The less hygroscopic group presented very low hygroscopicity κ_P values, between 0.032 and 0.068, while the values κ_P for the more hygroscopic group were low, and ranged between 0.110 and 0.172 (Rissler et al.,

10   2004, 2006) (Table S2 of Supplement). Here, the following classification by Gunthe et al. (2009) was considered: very low hygroscopicity (VLH, $\kappa_p < 0.1$), low hygroscopicity (LH, $0.1 \leq \kappa_p < 0.2$), medium hygroscopicity (MH, $0.2 \leq \kappa_p < 0.4$) and high hygroscopicity (HH, $\kappa_p \geq 0.4$). Neither set of observations included smoke particles with $\kappa_P > 0.2$. The hygroscopic group number fractions varied with very low hygroscopicity particles accounting for 20% of the total number concentration (Rissler et al., 2004), or up to 85% (Rissler et al., 2006) (Table S2 of supplement). As a result, the population

15   effective hygroscopicity parameter $\kappa_{p_{eff}}$ ranged between 0.05 and 0.13.

To assess the role of aerosol mixing state outside equilibrium conditions, cloud model simulations were conducted for populations both externally and internally mixed. The variability in the population effective $\kappa_{p_{eff}}$ was simulated assuming that the population is composed by two populations externally mixed in terms of hygroscopicity, having $\kappa_p = 0.04$ and $\kappa_p = 0.16$, respectively, with a resultant population effective hygroscopicity estimated as $\kappa_{p_{eff}} = \sum \kappa_{p,group} f_{group}$ (Gunthe et al.,

20   2009) that varies according to the number fraction f_{group} of each hygroscopic group (Table 2). This case is denoted *Ext1*. A second possibility, denoted *Ext2*, was considered to account for more hygroscopic biomass burning aerosols observed for other biomass/regions. In this second case, the κ_p of the more hygroscopic group is increased from $\kappa_p = 0.16$ to a medium hygroscopicity value, $\kappa_p = 0.30$, with a resultant population effective hygroscopicity also varying according to the number fraction of each hygroscopic group (Table 2). Finally, the internally mixed population was denoted *Int*. Results obtained for

25   two hygroscopic groups of particles externally mixed are compared with results obtained if the population is assumed to be internally mixed. The minimum/maximum κ_p in both sets of externally mixed populations is reached for the extreme case when only one group is present (therefore reducing to the internally mixed case) and is equal to the hygroscopicity parameter of particles in this group.

The effective $\kappa_{p_{eff}}$ and the corresponding fractions of each group for both situations and different fractions of the

30   hygroscopic groups are presented in Table 2. The schematic size distribution of the aerosol total population and that of the

hygroscopic group with $\kappa_p = 0.04$ are indicated in Fig. 1 for the three case studies, for a $\kappa_{p_{eff}} = 0.10$ and *Ext2* external mixing state. The aerosol composition was considered to be independent of particle size, assuming that the slight tendency of higher hygroscopicity of larger particles (Table S2 of supplement) was typically not large enough to impact significantly the CCN behavior of the population. Simulations were conducted for the internally mixed population (*Int*) with hygroscopicities that ranged from $\kappa_p = 0.02$ to $\kappa_p = 0.60$, for the defined MP$_{5,1}$, MP$_{1,5}$ and HP$_{5,5}$ cases, in order to analyze the effect of hygroscopicity. Simulations conducted for the externally mixed population (*Ext1* and *Ext2*) ranged between the minimum and maximum $\kappa_{p_{eff}}$ (0.04 to 0.16 and 0.04 to 0.30, respectively).

Updraft velocities between 0.1 m s^{-1} and 10 m s^{-1} were considered. Higher number concentrations than considered here can be found in pyrocumulus, but it is probably safe to assume that their impact on the hydrological cycle and aerosol indirect effect on a regional scale is secondary when compared with that of the regional haze, so these extreme cases of polluted conditions were not covered in our study. According to the regimes proposed by Reutter et al. (2009) (Sect. 2.5), our study focused largely on the aerosol-limited and aerosol- and updraft-sensitive regimes, with particle number concentrations that characterize polluted conditions like those found in the regional haze. For MP$_{5,1}$ and MP1,5 cases, the updraft limited case is given approximately by $W \leq 1$ m s^{-1}, but the aerosol-limited is given by $W \geq 6$ m s^{-1}. For the HP$_{5,5}$ case, the approximate limit of the updraft limited case is given by $W \leq 1$ m s^{-1}, and the aerosol-limited by $W \geq 10$ m s^{-1} (not considered in our simulations).

Cloud base initial conditions for the simulations were: temperature of 293 K, atmospheric pressure of 900 hPa and relative humidity of 98%. Sensitivity tests indicated only a weak dependence (absolute differences between maximum supersaturations obtained initializing at 80% and at 99% below 0.03%) of maximum supersaturations with the initial relative humidity for the highest updraft values, and a negligible effect in the activated fraction (See Figure S1 of Supplement). To avoid unrealistic physical parameters, the final time of simulation was defined somewhat arbitrarily as the time required for the parcel to ascend 500 m at the considered updraft velocity. The parameters for the simulations are summarized in Table 3. The distribution was discretized into 1000 bins ranged from 15 nm to 10^4 nm, leading to a relative error of less than 0.003% with respect to the log-normal distribution for all the cases considered in this study. To exclude particles that are not large enough to activate, only particles larger than 30 nm ($N_{a,30}$) were considered as aerosol number concentrations in the calculation of N_d / N_a fractions. For all the cases considered, the cloud nuclei larger than 30 nm fraction included almost all particles, with the lowest fraction $N_{a,total} / N_{a,30} = 0.994$ obtained for case MP$_{5,1}$.

4 Results and discussion

Maximum values of supersaturation and CCN activated fraction, as function of hygroscopicity, updraft velocity and mixing state, are presented in Fig. 2 for the various proposed case studies and mixing states. Due to the high particle number

concentrations that characterize polluted conditions in the three case studies, maximum supersaturations reached in the simulations were typically low and, except for the highest updraft velocities and for very low hygroscopicity values (VLH, $\kappa_p < 0.1$), with values that were below 0.5% in the MP$_{5,1}$ case, and below 0.4% in the MP$_{1,5}$ and HP$_{5,5}$ cases. The highest values of maximum supersaturation were obtained for the MP$_{5,1}$ case, with a majority of particles in the Aitken mode.

5 Maximum supersaturations in this case were, in average, ~ 0.10% larger (absolute differences) than those obtained for MP$_{1,5}$ case, and about 0.15% higher than those obtained for HP$_{5,5}$ case. Meanwhile, the values of maximum supersaturation reached in the MP$_{1,5}$ case study were higher than those obtained in the HP$_{5,5}$ case, but slightly, with absolute differences between maximum supersaturation values of up to 0.05%, all else being equal, in spite of the much higher particle number concentrations in the latter case. The case study with the highest N_a, HP$_{5,5}$, presented the largest cloud droplet number

10 concentrations. However, the largest N_d / N_a fractions were instead reached in the MP$_{1,5}$ case, all else being equal. The activated fractions for the HP$_{5,5}$ case were the lowest between all three cases for all values of κ_p within the low hygroscopicity (LH, $0.1 \leq \kappa_p < 0.2$) and medium hygroscopicity (MH, $0.2 \leq \kappa_p < 0.4$) ranges, while for κ_p in the VLH range the lowest N_d / N_a fractions were obtained for the MP$_{5,1}$ case.

These results for the maximum supersaturations and N_d / N_a fractions are explained by the Köhler theory, which predicts

15 that the Kelvin term typically dominates the growing process for larger particles, while the Raoult term is more relevant for smaller ones. Therefore, particles in the accumulation mode are likely to condense water vapor on their surfaces more readily than the comparatively smaller particles in the Aitken mode, growing larger and impacting more the maximum supersaturation reached than the latter. Moreover, the Raoult term is more significant the smaller the particle, thus the activation of particles in the Aitken mode is expected to be more altered by hygroscopicity than the activation of particles in

20 the accumulation mode.

Among the variable parameters within the simulations, both maximum supersaturations and N_d / N_a fractions were impacted the most by updraft velocity, for all study cases and mixing states. Mean sensitivities of N_d to W in the MP$_{5,1}$, MP$_{1,5}$ and HP$_{5,5}$ study cases were, respectively, 0.66, 0.65 and 0.73, with very little variability with mixing state, as illustrated in Fig. 3 for $\kappa_{p_{eff}} = 0.10$. These mean values of S_W are higher than previous estimations of 0.18 and 0.47 for clean (< 1000 cm^{-3}) and

25 polluted (1000 cm^{-3} to 3000 cm^{-3}) conditions, respectively, by McFiggans et al. (2006). Yet an increase of the sensitivity to W with the number concentration is consistent with the behavior expected within the updraft- and aerosol-sensitive regime that is, on average, the predominating regime. The adjusted R^2 coefficients in the linear fits of the $\ln(N_d)$ vs. $\ln(W)$ curves were ≥ 0.90 for all cases and mixing states. However, the data points departed from the mean slope towards low and high updraft velocities for all case studies and mixing states (Fig. 4, top). Cloud droplet number concentrations were more

30 sensitive (local S_W up to 0.9) to increases in the updraft velocity for velocities within the updraft-limited regime, while for

the aerosol-limited regime the sensitivity to W decreased to values between 0.1 and 0.4 (Fig. 4, bottom). This varying sensitivity of N_d to W is in agreement with the changing behavior within each regime of CCN activation described by Reutter et al. (2009), that varies from a high sensitivity of activation with W in the updraft-limited regime to almost no influence in the aerosol-limited one. The sensitivity of N_d to the aerosol number concentrations and the geometric mean diameter and standard deviation have been discussed elsewhere (McFiggans et al., 2006; Reutter et al., 2009) and was not addressed here.

In contrast with S_W, the sensitivity to hygroscopicity S_{κ_p} changed substantially with mixing state, and will be discussed in Sect. 4.3.

5.1 Aerosol mixing state

The aerosol mixing state modified both maximum supersaturations and activated fractions, although to different extents. The values of maximum supersaturation were slightly underestimated for updraft velocities in the aerosol-limited and the aerosol- and updraft-sensitive regimes when internal mixing was assumed (Fig. 2, top). The absolute differences were up to ~0.01 % and ~0.03 % for the externally mixed *Ext1* and *Ext2* populations, respectively. For updraft velocities within the updraft-limited regime, however, the maximum supersaturation reached were lowest, and the values assuming an internal mixing were almost identical or marginally higher than those reached for externally mixed populations.

On the other hand, the internal mixing hypothesis typically led to overestimations of N_d, regardless of the somewhat lower values of maximum supersaturation reached for this mixing case. The effect of hygroscopic mixing state in the CCN activation behavior of aerosols can be illustrated through the consideration of an aerosol population with known size and composition but no information on the mixing state. Particles in the externally mixed population will have either larger or smaller hygroscopicity parameters than that of the internally mixed population average. The more hygroscopic groups in the external mixture will have smaller cut particle diameters and will activate more readily than the internally mixed particles. Consequently, the number of more hygroscopic particles that become cloud droplets would be underestimated if internal mixing was presumed. Under the same assumption, the fraction of less hygroscopic particles that will be considered activated would be overestimated.

Although differences in activation for more and less hygroscopic particles due to internal mixing will contribute with opposite signs to the total N_d derived from mixing state, they are unlikely to cancel each other. In a simulation selected to illustrate the impact of mixing state in N_d, an externally mixed population (*Ext2*) have one hygroscopic group with $\kappa_p = 0.04$, in the VLH range, present in a fraction $f_{\kappa_p=0.04} = 0.77$, and a second hygroscopic group with $\kappa_p = 0.30$, within the MH range, with $f_{\kappa_p=0.30} = 0.23$. Assuming internal mixing (*Int*), these two groups resulted in $\kappa_{p_{eff}} = 0.10$ (Table 2). For this specific case, the schematic size distribution of particles that are activated as CCN in the MP$_{5,1}$, MP$_{1,5}$ and HP$_{5,5}$ case studies

at a prescribed updraft velocity of $W = 5$ m s^{-1} are presented for external and internal mixtures in Fig. 4. The values of maximum supersaturations reached were somewhat lower when internal mixing state was assumed, between 2% and 3% depending on the study case. A fraction of particles in the MH hygroscopic group ($\kappa_p = 0.30$) was indeed activated as CCN in the externally mixed *Ext2*, but was not in the internal mixing, since the internally mixed population $\kappa_{p_{eff}}$ is lower and thus

5   the cut size for activation in the internally mixed population is larger. However, an even larger fraction of the particles in the VLH group were not activated in the external mixing, but were considered as activated when internal mixing state was assumed. Thus, in this example, and characteristically in the conducted simulations, assuming internal mixing for an externally mixed population led to an overestimation of N_d.

Box plots on top of data in Fig. 5 display the magnitude of the overestimation in N_d if internal mixing is assumed for an

10   externally mixed population, for the range of updraft velocities and $\kappa_{p_{eff}}$. The overestimation of N_d was expressed as $N_{d,Int} / N_{d,Ext} - 1$, where $N_{d,Int}$ and $N_{d,Ext}$ refers to estimations for internally and externally mixed population, respectively, and the population is considered to be externally mixed. Overestimations of N_d when assuming internal mixing were larger when the module of the difference between the internal mixture $\kappa_{p_{eff}}$ and that of the hygroscopic group with closest value of hygroscopicity in the external mixture was greater, i.e. when the internally mixed assumption was comparatively less valid.

15   Overestimations close to the lower limit or below the interquartile range of CCN overestimations were obtained for populations with fractions $f_{\kappa=0.16} \geq 0.67$ in the *Ext1* (with a resulting $\kappa_{p_{eff}} \geq 0.12$), and $f_{\kappa=0.30} \geq 0.62$ in the *Ext2* mixing ($\kappa_{p_{eff}} \geq 0.2$). Within the aerosol- and updraft-sensitive regime, the overestimations of N_d were largest for all three cases. The higher number concentration of particles in the Aitken mode in the MP$_{5,1}$ and HP$_{5,5}$ case studies resulted in larger overestimations in the CCN number concentrations even for the upper range of updraft velocities. In contrast, the

20   overestimations of N_d decreased noticeably as the updraft velocity increased towards the aerosol-limited regime for the MP$_{1,5}$ case. Within the updraft-limited regime the typically low fractions of activated particles, as well as the estimations of $N_{d,Int} / N_{d,Ext} - 1$, were more susceptible to inaccuracies due to bin resolution.

Average overestimations of N_d for the externally mixed population *Ext1* were typically low, 5.7 ± 2.4 %, 5.1 ± 2.1 % and 2.9 ± 2.0 %, or the MP$_{5,1}$, MP$_{1,5}$ and HP$_{5,5}$ case studies. For population *Ext2*, and the same case studies, averages were

25   slightly higher, 12.4 ± 4.7 %, 10.4 ± 4.5 % and 10.5 ± 3.8 %, respectively. However, with particle number concentrations of 10 000 cm^{-3} in HP$_{5,5}$ case, and 6000 cm^{-3} in MP$_{5,1}$ and MP$_{1,5}$ case studies, the absolute overestimation ($N_{d,Int} - N_{d,Ext}$) in the CCN number concentration was, respectively, 160 ± 94 cm^{-3}, 181 ± 96 cm^{-3} and 224 ± 137 cm^{-3} for *Ext1* simulations and 349 ± 203 cm^{-3}, 358 ± 188 cm^{-3} and 467 ± 272 cm^{-3} for the *Ext2*. Maximum absolute overestimations were reached for higher updrafts, for which the N_d / N_a fraction was higher for all mixing states. For *Ext1* simulations, the maximum absolute

overestimations were 304 cm^{-3}, 323 cm^{-3} and 432 cm^{-3} for the MP$_{5,1}$, MP$_{1,5}$ and HP$_{5,5}$ cases, respectively, while in *Ext2* simulations for the same study cases they were of 637 cm^{-3}, 642 cm^{-3} and 838 cm^{-3}. The high aerosol number concentrations here considered, although characterize polluted conditions like those that could be found in regional hazes in the Amazonia region, are still moderate in comparison with concentrations inside pyro-cumulus.

5   It is important to note that, would the maximum supersaturations achieved in simulations for both mixing states be the same, N_d would be higher in the internal mixing case simulations and the CCN overestimations derived from assuming internal mixing would be larger. This difference in the achieved maximum supersaturations does not explains the much smaller impact of mixing state found for cloud parcel model results when compared to those obtained for equilibrium conditions and prescribed supersaturations, but is likely to contribute to it since, in the latter, the same maximum supersaturation is assumed

10 in the estimation of N_d for the different mixing states.

For Amazon smoke particles, these results indicate an overestimation in N_d derived from assuming internal mixing overestimation for an externally mixed population that is below 10% for all conditions.

4.2 Hygroscopicity

The behavior of the CCN activation, as hygroscopicity changed, was distinctly different for the different mixing states.

15 When the population was assumed to be internally mixed, the mean average sensitivity to hygroscopicity, S_{κ_p}, was low for the case MP$_{5,1}$ (0.20), and very low for MP$_{1,5}$ (0.10) and HP$_{5,5}$ (0.12) case studies. These estimations are in good agreement with those by Reutter et al. (2009) and Ward et al. (2010). For the externally mixed population, however, $\ln - \ln$ curves were far apart from a linear behavior and it was not possible to achieve linear fits. Obtained adjusted R^2 parameters were close to zero or negative and hence average sensitivities for externally mixed populations were not estimated.

20 Local sensitivities for the internal mixing state typically decreased as the hygroscopicity parameter increased, starting from median values of ~0.35 for the MP$_{5,1}$ case study and of ~0.20 for the MP$_{1,5}$ and HP$_{5,5}$ case studies (Fig. 7) until almost stabilizing at values close to 0.15, 0.05 and 0.10 for the same cases for values of κ_p within the medium and high hygroscopicity ranges. Notable exceptions were found within the updraft-limited regime for populations with high hygroscopicity where the impact of kinetic effects was high, as will be addressed later in Sect. 4.3. Except for cases within

25 the updraft-limited regime, were kinetic limitations were significant, we found that the impact of the hygroscopicity parameter in N_d was very low for internally mixed populations and κ_p within the MH or the HH ranges, while for $\kappa_{p_{eff}}$ values within the VLH range the impact was low to moderate, in agreement with results obtained by previous studies (Dusek et al., 2006; McFiggans et al., 2006; Reutter et al., 2009; Ward et al., 2010).

On the other hand, the local $S_{\kappa_{p_{eff}}}$ for the externally mixed populations presented mean values (over results for different

30 updraft velocities) that increased with $\kappa_{p_{eff}}$ from very low or even negative to values between 0.3 and 0.45 for the highest

$\kappa_{p_{eff}}$ values (Fig. 6). This higher sensitivity of N_d to $\kappa_{p_{eff}}$ in the external mixtures is also apparent in the step increase of N_d obtained for the external mixing results for the larger average $\kappa_{p_{eff}}$ values (Fig. 2, bottom).

The increasing $S_{\kappa_{p_{eff}}}$ for external mixing cases can be illustrated through the consideration of the following example for the HP$_{5,5}$ case and an updraft velocity $W = 5$ m s^{-1}. In the internally mixed population with $\kappa_p = 0.30$, 62% of the total N_a was

5 activated. If the internally mixed population has, instead, $\kappa_p = 0.25$, the resulting N_d / N_a fraction is ~61%. However, if the population with $\kappa_{p_{eff}} = 0.25$ is instead externally mixed, the fraction of particles with $\kappa_p = 0.30$ that reached activation increased to 67% but, of the particles with $\kappa_p = 0.04$ (19% of total population), only 22% reached activation. Consequently, even when the MH particles predominated, the resulting N_d / N_a ratio was 58%, a more significant decrease from the case with $\kappa_p = 0.30$ than in the internally mixed population case.

10 Considering the results from the simulations and the little variability and low values of $S_{\kappa_{p_{eff}}}$ for internally mixed populations, variations of hygroscopicity within the MH and HR could be considered as rather secondary and neglected, especially if the difference in hygroscopicity is not large, since the level of sophistication within GCMs should be kept at minimum whenever the accuracy of results is not compromised. When the hygroscopicity is within the LH and VLH, however, the overestimation in the activated fraction might be substantial as illustrated in Fig. 7 for updraft velocities in the

15 updraft- and aerosol sensitive regime, also for internally mixed populations. In the extreme case when $\kappa_p = 0.20$ was assumed for a population of $\kappa_p = 0.04$, the mean overestimation of the CCN population for the MP$_{5,1}$, MP$_{1,5}$ and HP$_{5,5}$ was, respectively, 54.3 ± 3.7 %, 22.4 ± 1.4 % and 26.6 ± 2,3 %. In comparison, if $\kappa_p = 0.60$ was presumed for aerosols with $\kappa_p = 0.20$, the mean overestimations of N_d obtained for the MP$_{5,1}$, MP$_{1,5}$ and HP$_{5,5}$ cases and the same range of updraft velocities were, respectively, 15.5 ± 1.6 %, 4.8 ± 0.3 % and 6.4 ± 0.8%.

20 A significant overestimation of N_d can thus result from assuming an hygroscopicity in the MH range for the Amazon smoke aerosols. These results suggest that larger values of κ_p like those recommended for continental aerosol or biomass burning particles in other regions of the world are not adequate to describe the CCN activation behavior of Amazon smoke particles.

4.3 Kinetic limitations

Temporal series of the CCN activation with resolutions of 0.5 s and 1 s near the time of maximum supersaturation for strong

25 and low to moderate updrafts, respectively, were used to analyze the particle growth and activation evolution in time. Three separate effects in the evolution of N_d observed in the simulations for weak and sometimes even moderate updrafts that could be attributed to the effect of kinetic limitations: (1) a delay between the time when maximum supersaturation was

reached and the time when the activated fraction is largest; (2) a decrease in the number of activated particles with cloud depth after the maximum activated fraction is reached; and finally, (3) a overestimation of N_d if assuming that equilibrium applies.

The delay in activation was amplified with the increase of the particle $\kappa_{p_{eff}}$. A relation to particle size and number concentration was also apparent, being the delay longest for the $HP_{5,5}$ case, moderate in the $MP_{1,5}$ case, and much shorter for the $MP_{5,1}$ case, also for large $\kappa_{p_{eff}}$ values and weak updrafts. This is illustrated in Fig. 8 for an internally mixed population and $W = 0.5$ m s^{-1}. Due to the delay in activation, typically, a significant fraction of particles was not activated at the time maximum supersaturation was reached. Within the updraft-limited regime, the delay in the activation was such that at the time of maximum supersaturation no particles are activated for internally mixed populations with $\kappa_{p_{eff}}$ above a certain threshold. For an updraft velocity of $W = 0.5$ m s^{-1}, this threshold was $\kappa_{p_{eff}} = 0.50$ for the $MP_{5,1}$ case and $\kappa_{p_{eff}} = 0.35$ for the $MP_{1,5}$ and $HP_{5,5}$ case, respectively. In the $MP_{1,5}$ case, for an updraft velocity $W = 3$ m s^{-1}, already in the updraft- and aerosol sensitive regime, the threshold was still $\kappa_{p_{eff}} = 0.35$. The maximum value of N_{d,neq_simp} was also reached sometime after the maximum supersaturation is reached, and its value was slightly higher than the maximum of $N_{d,neq}$. However, strong kinetic effects obtained for the larger $\kappa_{p_{eff}}$ values near the time of maximum supersaturation for $N_{d,neq}$ were not so strong for N_{d,neq_simp}. After the maximum $N_{d,neq}$ is reached, however, differences between both estimations are below 1% and at the end of the simulation both estimations are very similar. The fraction of particles not strictly activated in $N_{d,neq}$ was important only near the time of maximum supersaturation, indicating that this assumption has no influence in results presented in previous sections, were cloud droplet concentrations were estimated at the end of the simulation. However, the differences near the time of maximum supersaturation would be larger if this fraction is disregarded.

For the externally mixed population *Ext1*, although $N_{d,neq}$ was significantly lower than $N_{d,eq}$ for weak updrafts, in all the cases at least a fraction of particles was activated at the time of maximum supersaturation. For *Ext2* and $W = 0.5$ m s^{-1}, however, populations with $\kappa_{p_{eff}} \geq 0.12$, or $f_{\kappa_p=0.30} \geq 0.31$, also showed $N_{d,neq} = 0$ for both $MP_{1,5}$ and $HP_{5,5}$ cases at the time of maximum supersaturation. This is exemplified in the Fig. 9 for three values of the effective hygroscopicity parameter. Interestingly enough, particles from both hygroscopic groups failed to activate in these conditions. The value of maximum supersaturation was very low in these cases and it is likely that particles in the more hygroscopic group condense the limited water vapor on their surfaces more readily, although not in enough quantities as to activate themselves, but limiting even more the water vapor available to less hygroscopic particles and preventing their activation as well. Particles from both groups seem to grow rather slowly and both groups appear to activate at the same time.

As moderate and strong updrafts were considered, the delay between maximum supersaturation and maximum activation reduced until no longer observed at the temporal resolution of the time series. Within the updraft limited regime, the mean overestimation of $N_{d,neq}$ in comparison with $N_{d,eq}$ over the range of $\kappa_{p_{eff}}$, excluding those that led to $N_{d,neq} = 0$, ranged from ~10% to ~100% in internally mixed populations, and between ~10% to ~250% in externally mixed ones (Fig. 10), being larger for the higher values of $\kappa_{p_{eff}}$. However, for all case studies and mixing states, the overestimation at the time of maximum supersaturation was typically below 12% within the updraft- and aerosol-sensitive, and below 5% within the aerosol-limited regime .

The overestimation of $N_{d,neq}$ at the time of maximum supersaturation if assuming equilibrium applies can be explained by the evaporation mechanism. Yet, as the cloud depth increases, and in particular at the defined end of the simulation, the deactivation mechanism can be more relevant. Although $N_{d,neq}$ was always lower at the end of the simulation that at its maximum, the difference was typically low, between 2% and 10% for most updraft velocities and mixing states, as evidenced in the similar the overestimations of both values by $\max(N_{d,eq})$. Both evaporation and deactivation mechanisms were relevant for weak and even moderate updrafts, and a relation with particle size and number concentration was apparent, as previously reported by Nenes et al. (2001) for ammonium sulfate particles (2001). Our results are also consistent with the reduction in the droplet concentrations of up to 35% kinetic limitations found by Roberts et al. (2003) for updrafts of 0.1 ms^{-1} and aerosol data corresponding to the dry season in Amazonia.

In our results, the effects of kinetic limitations were strong when a significant fraction of particles with hygroscopicity in the MH or LH range was present. However, for particles with low and very low hygroscopicities like the Amazon smoke particles, kinetic limitations were less important, even if large aerosol loads were present.

A relation between the time scale of solubility and the CCN activation behavior of aerosols has been known (Chuang, 2006) and several studies have analyzed kinetic limitations comparing the aerosol particles grow and that of a calibration aerosol with a high solubility and the same critical supersaturation, with mixed conclusions regarding the importance of this process to CCN activation (Bougiatioti et al., 2011; Engelhart et al., 2008; Padró et al., 2012; Raatikainen et al., 2012; Ruehl et al., 2007). However, at the low supersaturations reached as a result of the weak updraft velocity and the large aerosol loads considered, the kinetic limitations discussed in this study derive more likely from the differences in water uptake and critical supersaturation due to the particle hygroscopicity.

5 Conclusions

The available data on smoke particles in the Amazon region (Sect. 3) suggest that that this aerosol population has a rather consistent size and that external mixing of two particle groups having very low and low hygroscopicity, respectively, is typical for this aerosol population. We conducted cloud model simulations using three hypothetical case studies and a variety

of hygroscopicities and mixing states that resembled typical conditions found in the literature for smoke aerosols in the Amazon in moderate to highly polluted conditions. Simulations were conducted for these three case studies to estimate the effect of different values of hygroscopicity and mixing state, including those conditions that resemble observed data for smoke particles (*Ext1*). The impact of kinetic limitations was assessed.

5   The impact in the surface tension due to the organic material present in smoke aerosols is likely to be relevant (Fors et al., 2010; Giordano et al., 2013), but was not included in this work due to the complex organic composition of these particles that lead to difficulties for its modelling. We address that this is a limitation of our results and should be addressed in future works.

A low sensitivity of the cloud droplet number concentration N_d to the population effective hygroscopicity parameter $\kappa_{p_{eff}}$

10   was found for medium and large hygroscopicity when the population was internally mixed. Yet, for particles with hygroscopicity in the lower range of $\kappa_{p_{eff}}$ (< 0.20) the effective hygroscopicity of smoke particles for the Amazon appears

to stand in the VLH and LH ranges, where the sensitivity to this parameter was found to be moderate. Therefore N_d could be overestimated significantly if larger values of hygroscopicity, like those suggested for biomass burning particles elsewhere, were to be used for Amazonia smoke particles.

15   Hygroscopic mixing state in the conducted cloud model simulations led to differences lower than those obtained in previous studies that addressed mixing state for equilibrium conditions and prescribed supersaturations. In particular, the overestimation of N_d was low for populations similar in hygroscopicity to the Amazon smoke aerosols (*Ext1* in the simulations), but slightly higher when the external mixing was between groups with VLH and MH (*Ext2*).

The $\kappa_{p_{eff}}$ parameter posed a much larger impact on the CCN activation within the MH range for externally mixed

20   populations than for internally mixed ones, even for low fractions of VLH aerosols. When $\kappa_{p_{eff}}$ is estimated assuming internal mixing, and in particular when particles of VLH are present, it is important to take into account that the typically low sensitivity to hygroscopicity of internally mixed populations does not apply and even relatively small variabilities in $\kappa_{p_{eff}}$ could affect the CCN activation behavior of the population. Consequently, assuming internal mixing of particles with very low and low hygroscopicity particles with moderate or large hygroscopicity should be avoided.

25   Finally, kinetic limitations were found to be much lower for particles within VLH and LH hygroscopic groups and, therefore, its impact on the CCN behavior of Amazon smoke particles is expected to be limited, in spite of the presence of large aerosol loads.

The inclusion of mixing state, adequate hygroscopicity values and the consideration of kinetic limitations into global and regional circulation model are all possible, although in many cases at a computational cost. The choice of to use two separate

30   aerosol populations to account for the externally mixing character of the biomass burning population will increase the computational burden of the model and the modeler might choose instead to consider biomass burning aerosols as only one

population internally mixed and externally mixed with other aerosol populations, given that the overestimation derived from this choice is not significant. Global models or regional models over a large domain should specify if possible the aerosol hygroscopicity for different regions, in particular when values in the very low or low range of hygroscopicity are to be considered. Also for Amazonia smoke aerosols, the choice of a parameterization that accounts for kinetic limitations, typically more demanding in terms of computational resources, might not improve results significantly over a parameterization that don't account for their impact.

Appendix A: Nomenclature of frequently used symbols

CCN Cloud condensation nuclei

N_d Cloud droplet number concentration

N_a Aerosol number concentration

$N_{d,eq}$ CD estimated assuming equilibrium conditions

$N_{d,neq}$ CD estimated without assuming equilibrium conditions

$d_{dry,c}$ particle cut diameter for activation (dry)

f_{hg} number fraction of hygroscopic group h

S_{X_i} sensitivity of CD to the parameter χ_i

s supersaturation

S_{max} cloud maximum supersaturation

t time

T temperature

W cloud parcel updraft velocity

κ_P specific hygroscopicity parameter by Petter & Kreidenweis (2007)

$\kappa_{P_{eff}}$ population effective specific hygroscopicity parameter

Appendix B: Simplified Köhler equation and estimation of the cut diameter for CCN activation

For an aerosol particle with dry diameter d_{dry} and formed by a soluble fraction and an insoluble core, the Köhler equation can be approximated by the expression (Pruppacher and Klett, 1997):

$$S \approx 1 + \frac{A}{d} - \frac{B d_{dry}^3}{d^3 - d_{dry}^3} \tag{B1}$$

where s is the supersaturation, d is the particle wet diameter, and terms A and B are parameters in the curvature and solute terms of the Köhler equation. In this work, B was assumed to be identical to the parameter κ_P for all values of κ_p and S_c.

It can be showed (Pruppacher and Klett, 1997) that the particle cut wet diameter for activation d_c can be estimated as:

$$d_c = -D + \left(D^2 - E\right)^{1/2} \tag{B2}$$

where the parameters D and E are estimated as:

$$D = \frac{B^2 A - 3 B A s}{3 B s^2 - 3 B^2 s} \tag{B3}$$

and

$$E = \frac{3 B A^2}{3 B s^2 - 3 B^2 s} \tag{B4}$$

Finally, the corresponding dry diameter of the smallest activated particle, $d_{dry,c}$, can be calculated as:

$$d_{dry,c}^3 = \frac{d_c^3 (A - s d_c)}{A + (B - s) d_c} \tag{B5}$$

Acknowledgements

The authors thank anonymous referees 1 and 2 for their valuable suggestions and comments that contributed significantly to the improvement of the present manuscript. This work was supported by the São Paulo Research Foundation (FAPESP), through the projects 2012/13575-9, DR 2012/09934-3, BEPE 2013/02101-9 and BPE 2014/01564-8.

References

Abdul-Razzak, H. and Ghan, S.: A parameterization of aerosol activation: 2. Multiple aerosol types, J. Geophys. Res., 105, 6837–6844, 2000.

Abdul-Razzak, H. and Ghan, S. J.: A parameterization of aerosol activation: 3. Sectional representation, J. Geophys. Res, 107, 1–6 [online] Available from: http://www.agu.org/journals/jd/jd0203/2001JD000483/1.shtml (Accessed 16 April 2012), 2002.

Almeida, G. P., Brito, J., Morales, C. A., Andrade, M. F. and Artaxo, P.: Measured and modelled cloud condensation nuclei (CCN) concentration in São Paulo, Brazil: The importance of aerosol size-resolved chemical composition on CCN concentration prediction, Atmos. Chem. Phys., 14(14), 7559–7572, doi:10.5194/acp-14-7559-2014, 2014.

Andreae, M. O.: Biomass burning: It's history, use, and distribution and it's impact on environmental quality and global climate, in Global biomass Burning: Atmospheric, Climatic and Biospheric Implications, edited by J. S. Levine, pp. 3–21,

MIT Press, Cambridge, Massachussets., 1991.

Andreae, M. O., Artaxo, P., Fischer, H., Freitas, S. R., Grégoire, J.-M., Hansel, A., Hoor, P., Kormann, R., Krejci, R., Lange, L., Lelieveld, J., Lindinger, W., Longo, K., Peters, W., de Reus, M., Scheeren, B., Silva Dias, M. a. F., Ström, J., van Velthoven, P. F. J. and Williams, J.: Transport of biomass burning smoke to the upper troposphere by deep convection in the equatorial region, Geophys. Res. Lett., 28(6), 951–954, doi:10.1029/2000GL012391, 2001.

Andreae, M. O., Rosenfeld, D., Artaxo, P., Costa, A. A., Frank, G. P., Longo, K. M. and Silva-Dias, M. A. F.: Smoking rain clouds over the Amazon., Science (80-.)., 303, 1337–1342, doi:10.1126/science.1092779, 2004.

Artaxo, P., Rizzo, L. V., Brito, J. F., Barbosa, H. M. J., Arana, A., Sena, E. T., Cirino, G. G., Bastos, W., Martin, S. T. and Andreae, M. O.: Atmospheric aerosols in Amazonia and land use change: from natural biogenic to biomass burning conditions, Faraday Discuss., doi:10.1039/c3fd00052d, 2013.

Ban-weiss, G. A., Jin, L., Bauer, S. E., Bennartz, R., Liu, X., Zhang, K., Ming, Y., Guo, H. and Jiang, J. H.: Journal of Geophysical Research : Atmospheres, , (December 2014), 876–901, doi:10.1002/2014JD021722.Received, 2014.

Bauer, S. E. and Menon, S.: Aerosol direct, indirect, semidirect, and surface albedo effects from sector contributions based on the IPCC AR5 emissions for preindustrial and present-day conditions, J. Geophys. Res. Atmos., 117, 1–15, doi:10.1029/2011JD016816, 2012.

Bauer, S. E., Menon, S., Koch, D., Bond, T. C. and Tsigaridis, K.: A global modeling study on carbonaceous aerosol microphysical characteristics and radiative effects, Atmos. Chem. Phys., 10(15), 7439–7456, doi:10.5194/acp-10-7439-2010, 2010.

Bougiatioti, A., Nenes, A., Fountoukis, C., Kalivitis, N., Pandis, S. N. and Mihalopoulos, N.: Size-resolved CCN distributions and activation kinetics of aged continental and marine aerosol, Atmos. Chem. Phys., 11(16), 8791–8808, doi:10.5194/acp-11-8791-2011, 2011.

Brito, J., Rizzo, L. V., Morgan, W. T., Coe, H., Johnson, B., Haywood, J., Longo, K., Freitas, S., Andreae, M. O. and Artaxo, P.: Ground based aerosol characterization during the South American Biomass Burning Analysis (SAMBBA) field experiment, Atmos. Chem. Phys., 14, 12069–12083, doi:10.5194/acp-14-12069-2014, 2014.

Camponogara, G., Silva Dias, M. A. F. and Carrió, G. G.: Relationship between Amazon biomass burning aerosols and rainfall over the La Plata Basin, Atmos. Chem. Phys., 14(9), 4397–4407, doi:10.5194/acp-14-4397-2014, 2014.

Carrico, C. M., Petters, M. D., Kreidenweis, S. M., Sullivan, A. P., McMeeking, G. R., Levin, E. J. T., Engling, G., Malm, W. C. and Collett Jr., J. L.: Water uptake and chemical composition of fresh aerosols generated in open burning of biomass, Atmos. Chem. Phys., 10(11), 5165–5178, doi:10.5194/acp-10-5165-2010, 2010.

Christensen, S. I. and Petters, M. D.: The role of temperature in cloud droplet activation., J. Phys. Chem. A, 116(39), 9706–17, doi:10.1021/jp3064454, 2012.

Chuang, P. Y.: Sensitivity of cloud condensation nuclei activation processes to kinetic parameters, J. Geophys. Res., 111(9), 1–7, doi:10.1029/2005JD006529, 2006.

Crutzen, P. J. and Andreae, M. O.: Biomass burning in the tropics: impact on atmospheric chemistry and biogeochemical

cycles., Science, 250(4988), 1669–78, doi:10.1126/science.250.4988.1669, 1990.

Cubison, M. J., Ervens, B., Feingold, G., Docherty, K. S., Ulbrich, I. M., Shields, L., Prather, K., Hering, S. and Jimenez, J. L.: The influence of chemical composition and mixing state of Los Angeles urban aerosol on CCN number and cloud properties, Atmos. Chem. Phys., 8, 5649–5667, doi:10.5194/acpd-8-5629-2008, 2008.

5 Dusek, U., Frank, G. P., Hildebrandt, L., Curtius, J., Schneider, J., Walter, S., Chand, D., Drewnick, F., Hings, S., Jung, D., Borrmann, S. and Andreae, M. O.: Size matters more than chemistry for cloud-nucleating ability of aerosol particles., Science (80-.)., 312(5778), 1375–8, doi:10.1126/science.1125261, 2006.

Dusek, U., Frank, G. P., Massling, A., Zeromskiene, K., Iinuma, Y., Schmid, O., Helas, G., Hennig, T., Wiedensohler, A. and Andreae, M. O.: Water uptake by biomass burning aerosol at sub- and supersaturated conditions: closure studies and

10 implications for the role of organics, Atmos. Chem. Phys., 11(18), 9519–9532, doi:10.5194/acp-11-9519-2011, 2011.

Engelhart, G. J., Asa-Awuku, a., Nenes, a. and Pandis, S. N.: CCN activity and droplet growth kinetics of fresh and aged monoterpene secondary organic aerosol, Atmos. Chem. Phys., 8(14), 3937–3949, doi:10.5194/acp-8-3937-2008, 2008.

Engelhart, G. J., Hennigan, C. J., Miracolo, M. a., Robinson, a. L. and Pandis, S. N.: Cloud condensation nuclei activity of fresh primary and aged biomass burning aerosol, Atmos. Chem. Phys., 12, 7285–7293, doi:10.5194/acp-12-7285-2012,

15 2012.

Ervens, B., Cubison, M. J., Andrews, E., Feingold, G., Ogren, J. a., Jimenez, J. L., Quinn, P. K., Bates, T. S., Wang, J., Zhang, Q., Coe, H., Flynn, M. and Allan, J. D.: CCN predictions using simplified assumptions of organic aerosol composition and mixing state: a synthesis from six different locations, Atmos. Chem. Phys., 10(10), 4795–4807, doi:10.5194/acp-10-4795-2010, 2010.

20 Farmer, D. K., Cappa, C. D. and Kreidenweis, S. M.: Atmospheric Processes and Their Controlling Influence on Cloud Condensation Nuclei Activity, Chem. Rev., 150313151440005, doi:10.1021/cr5006292, 2015.

Feingold, G.: Modeling of the first indirect effect: Analysis of measurement requirements, Geophys. Res. Lett., 30(19), 1–4, doi:10.1029/2003GL017967, 2003.

Fors, E. O., Rissler, J., Massling, A., Svenningsson, B., Andreae, M. O., Dusek, U., Frank, G. P., Hoffer, A., Bilde, M., Kiss,

25 G., Janitsek, S., Henning, S., Facchini, M. C., Decesari, S. and Swietlicki, E.: Hygroscopic properties of Amazonian biomass burning and European background HULIS and investigation of their effects on surface tension with two models linking H-TDMA to CCNC data, Atmos. Chem. Phys., 10(12), 5625–5639, doi:10.5194/acp-10-5625-2010, 2010.

Freitas, S. R., Longo, K. M., Silva Dias, M. A. F., Silva Dias, P. L., Chatfield, R., Prins, E., Artaxo, P., Grell, G. A. and Recuero, F. S.: Monitoring the transport of biomass burning emissions in South America, Environ. Fluid Mech., 5(1–2),

30 135–167, doi:10.1007/s10652-005-0243-7, 2005.

Fromm, M. D. and Servranckx, R.: Transport of forest fire smoke above the tropopause by supercell convection, Geophys. Res. Lett., 30, 1–4, doi:10.1029/2002GL016820, 2003.

Ghan, S. J., Abdul-Razzak, H., Nenes, A., Ming, Y., Liu, X., Ovchinnikov, M., Shipway, B., Meskhidze, N., Xu, J. and Shi, X.: Droplet nucleation: Physically-based parameterizations and comparative evaluation, J. Adv. Model. Earth Syst., 3(10),

1–33, doi:10.1029/2011MS000074, 2011.

Giordano, M. R., Short, D. Z., Hosseini, S., Lichtenmerg, W. and Asa-Awuku, A. A.: Changes in droplet surface tension affect the observed hygroscopicity of photochemically aged biomass burning aerosol., Environ. Sci. Technol., 47(3), 10980–10986, doi:10.1021/es404971u, 2013.

5 Gunthe, S. S., King, S. M., Rose, D., Chen, Q., Roldin, P., Farmer, D. K., Jimenez, J. L., Artaxo, P., Andreae, M. O., Martin, S. T. and Pöschl, U.: Cloud condensation nuclei in pristine tropical rainforest air of Amazonia: size-resolved measurements and modeling of atmospheric aerosol composition and CCN activity, Atmos. Chem. Phys., 9(1), 7551–7575, doi:10.5194/acpd-9-3811-2009, 2009.

He, J., Zhang, Y., Glotfelty, T., He, R., Bennartz, R., Rausch, J. and Sartelet, K.: Decadal simulation and comprehensive

10 evaluation of CESM/CAM5.1 with advanced chemistry, aerosol microphysics, and aerosol-cloud interactions, J. Adv. Model. Earth Syst., 7, 110–141, doi:10.1002/2014MS000360, 2015.

Hindmarsh, A. C.: The PVODE and IDA algorithms., 2000.

Hindmarsh, A. C. and Taylor, A. G.: User Documentatin of IDA, a differential-algebraic equation solver for sequential and parallel computers., 1999.

15 Hsiao, T.-C., Ye, W.-C., Wang, S.-H., Tsay, S.-C., Chen, W.-N., Lin, N.-H., Lee, C.-T., Hung, H.-M., Chuang, M.-T. and Chantara, S.: Investigation of the CCN Activity, BC and UVBC Mass Concentrations of Biomass Burning Aerosols during the 2013 BASELInE Campaign, Aerosol Air Qual. Res., doi:10.4209/aaqr.2015.07.0447, 2016.

Hudson, J. G.: Variability of the relationship between particle size and cloud-nucleating ability, Geophys. Res. Lett., 34(8), 1–5, doi:10.1029/2006GL028850, 2007.

20 IPCC: Climate Change 2013: The Physical Science Basis. Contribution of Working Group I to the Fifth Assessment Report of the Intergovernmental Panel on Climate Change, edited by V. B. and P. M. M. (eds. . Stocker, T.F., D. Qin, G.-K. Plattner, M. Tignor, S.K. Allen, J. Boschung, A. Nauels, Y. Xia, Cambridge University Press, Cambridge, United Kingdom and New York, NY, USA., 2013.

Jacobson, M.: The short-term cooling but long-term global warming due to biomass burning, J. Clim., 17, 2909–2926, 2004.

25 Jacobson, M. Z.: Fundamentals of atmospheric modeling, 2nd ed., Cambridge University Press, Cambridge, Massachussets., 2005.

Kandler, K. and Schütz, L.: Climatology of the average water-soluble volume fraction of atmospheric aerosol, Atmos. Res., 83(1), 77–92, doi:10.1016/j.atmosres.2006.03.004, 2007.

Köhler, H.: The nucleus in and the growth of hygroscopic droplets, Trans. Faraday Soc., 32, 1152–1161, 1936.

30 Langmann, B., Duncan, B., Textor, C., Trentmann, J. and Vanderwerf, G.: Vegetation fire emissions and their impact on air pollution and climate, Atmos. Environ., 43(1), 107–116, doi:10.1016/j.atmosenv.2008.09.047, 2009.

Lathem, T. L., Beyersdorf, A. J., Thornhill, K. L., Winstead, E. L., Cubison, M. J., Hecobian, A., Jimenez, J. L., Weber, R. J., Anderson, B. E. and Nenes, A.: Analysis of CCN activity of Arctic aerosol and Canadian biomass burning during summer 2008, Atmos. Chem. Phys., 13, 2735–2756, doi:10.5194/acp-13-2735-2013, 2013.

Longo, K. M., Freitas, S. R., Andreae, M. O., Setzer, A., Prins, E. and Artaxo, P.: The Coupled Aerosol and Tracer Transport model to the Brazilian developments on the Regional Atmospheric Modeling System (CATT-BRAMS) – Part 2: Model sensitivity to the biomass burning inventories, Atmos. Chem. Phys., 10(13), 5785–5795, doi:10.5194/acp-10-5785-2010, 2010.

5 Makkonen, R., Seland, O., Kirkevag, A., Iversen, T. and Kristjánsson, J. E.: Evaluation of aerosol number concentrations in NorESM with improved nucleation parameterization, Atmos. Chem. Phys., 14(10), 5127–5152, doi:10.5194/acp-14-5127-2014, 2014.

McFiggans, G., Artaxo, P., Baltensperger, U., Coe, H., Facchini, M. C., Feingold, G., Fuzzi, S., Gysel, M., Laaksonen, A., Lohmann, U., Mentel, T. F., Murphy, D. M., O'Dowd, C. D., Snider, J. R. and Weingartner, E.: The effect of physical and
10 chemical aerosol properties on warm cloud droplet activation, Atmos. Chem. Phys, 6, 2593–2649, 2006.

Mircea, M., Facchini, M. C., Decesari, S., Cavalli, F., Emblico, L., Fuzzi, S., Vestin, A., Rissler, J., Swietlicki, E., Frank, G., Andreae, M. O., Maenhaut, W., Rudich, Y. and Artaxo, P.: Importance of the organic aerosol fraction for modeling aerosol hygroscopic growth and activation: a case study in the Amazon Basin, Atmos. Chem. Phys., 5, 3111–3126, 2005.

Nenes, A., Ghan, S., Abdul-Razzak, H., Chuang, P. Y. and Seinfeld, J. H.: Kinetic limitations on cloud droplet formation and
15 impact on cloud albedo, Tellus B, 53(2), 133–149, doi:10.1034/j.1600-0889.2001.d01-12.x, 2001.

Padró, L. T., Moore, R. H., Zhang, X., Rastogi, N., Weber, R. J. and Nenes, A.: Mixing state and compositional effects on CCN activity and droplet growth kinetics of size-resolved CCN in an urban environment, Atmos. Chem. Phys., 12(21), 10239–10255, doi:10.5194/acp-12-10239-2012, 2012.

Petters, M. D., Carrico, C. M., Kreidenweis, S. M., Prenni, A. J., DeMott, P. J., Collett, J. L. and Moosmüller, H.: Cloud
20 condensation nucleation activity of biomass burning aerosol, J. Geophys. Res., 114(D22), D22205, doi:10.1029/2009JD012353, 2009.

Phinney, L. A., Lohmann, U. and Leaitch, W. R.: Limitations of using an equilibrium approximation in an aerosol activation parameterization, J. Geophys. Res., 108(D12), 4371, doi:10.1029/2002JD002391, 2003.

Pierce, J. R., Croft, B., Kodros, J. K., D'Andrea, S. D. and Martin, R. V.: The importance of interstitial particle scavenging
25 by cloud droplets in shaping the remote aerosol size distribution and global aerosol-climate effects, Atmos. Chem. Phys., 15(11), 6147–6158, doi:10.5194/acp-15-6147-2015, 2015.

Pringle, K. J., Tost, H., Pozzer, A., Pöschl, U. and Lelieveld, J.: Global distribution of the effective aerosol hygroscopicity parameter for CCN activation, Atmos. Chem. Phys., 10(12), 5241–5255, doi:10.5194/acp-10-5241-2010, 2010.

Pruppacher, H. R. and Klett, J. D.: Microphysics of Clouds and Precipitation, 2nd ed., Springer Netherlands, Dordrecht.,
30 1997.

Raatikainen, T., Moore, R. H., Lathem, T. L. and Nenes, A.: A coupled observation - Modeling approach for studying activation kinetics from measurements of CCN activity, Atmos. Chem. Phys., 12(9), 4227–4243, doi:10.5194/acp-12-4227-2012, 2012.

Ramanathan, V.: Aerosols, Climate, and the Hydrological Cycle, Science (80-.)., 294(5549), 2119–2124,

doi:10.1126/science.1064034, 2001.

Reid, J. S., Hobbs, P. V., Ferek, R. J., Blake, D. R., Martins, J. V., Dunlap, M. R. and Liousse, C.: Physical, chemical, and optical properties of regional hazes dominated by smoke in Brazil, J. Geophys. Res, 103(98), 1998.

Reutter, P., Su, H., Trentmann, J., Simmel, M., Rose, D., Gunthe, S. S., Wernli, H., Andreae, M. O. and Pöschl, U.: Aerosol- and updraft-limited regimes of cloud droplet formation: influence of particle number, size and hygroscopicity on the activation of cloud condensation nuclei (CCN), Atmos. Chem. Phys., 9(18), 7067–7080, doi:10.5194/acp-9-7067-2009, 2009.

Rissler, J., Swietlicki, E., Zhou, J., Roberts, G., Andreae, M. O., Gatti, L. V. and Artaxo, P.: Physical properties of the sub-micrometer aerosol over the Amazon rain forest during the wet-to-dry season transition – comparison of modeled and measured CCN concentrations, Atmos. Chem. Phys, 4, 2119–2143, 2004.

Rissler, J., Vestin, A., Swietlicki, E., Fisch, G., Zhou, J., Artaxo, P. and Andreae, M. O.: Size distribution and hygroscopic properties of aerosol particles from dry-season biomass burning in Amazonia, Atmos. Chem. Phys, 471–491, 2006.

Rissman, T. A., Nenes, A. and Seinfeld, J. H.: Chemical amplification (or dampening) of the Twomey effect: Conditions derived from droplet activation theory., J. Atmos. Sci., 61, 919–930, 2004.

Roberts, G. C., Nenes, A., Seinfeld, J. H. and Andreae, M. O.: Impact of biomass burning on cloud properties in the Amazon Basin, J. Geophys. Res., 108(D2), 4062, doi:10.1029/2001JD000985, 2003.

Rosário, N. E., Longo, K. M., Freitas, S. R., Yamasoe, M. A. and Fonseca, R. M.: Modeling the South American regional smoke plume: Aerosol optical depth variability and surface shortwave flux perturbation, Atmos. Chem. Phys., 13, 2923–2938, doi:10.5194/acp-13-2923-2013, 2013.

Rose, D., Nowak, A., Achtert, P., Wiedensohler, A., Hu, M., Shao, M., Zhang, Y., Andreae, M. O. and Pöschl, U.: Cloud condensation nuclei in polluted air and biomass burning smoke near the mega-city Guangzhou, China – Part 1: Size-resolved measurements and implications for the modeling of aerosol particle hygroscopicity and CCN activity, Atmos. Chem. Phys., 10(7), 3365–3383, doi:10.5194/acp-10-3365-2010, 2010.

Ruehl, C. R., Chuang, P. Y. and Nenes, A.: How quickly do cloud droplets form on atmospheric particles?, Atmos. Chem. Phys. Discuss., 7(5), 14233–14264, doi:10.5194/acpd-7-14233-2007, 2007.

Seinfeld, J. H. and Pandis, S. N.: Atmospheric Chemistry and Physics: From Air Pollution to Climate Change, 2nd ed., Wiley Interscience, New Jersey., 2006.

Swietlicki, E., Hansson, H.-C., Hämeri, K., Svenningsson, B., Massling, A., Mcfiggans, G., Mcmurry, P. H., Petäjä, T., Tunved, P., Gysel, M., Topping, D., Weingartner, E., Baltensperger, U., Rissler, J., Wiedensohler, A. and Kulmala, M.: Hygroscopic properties of submicrometer atmospheric aerosol particles measured with H-TDMA instruments in various environments—a review, Tellus B, 60B, 432–469, doi:10.1111/j.1600-0889.2008.00350.x, 2008.

Tosca, M. G., Randerson, J. T. and Zender, C. S.: Global impact of smoke aerosols from landscape fires on climate and the Hadley circulation, Atmos. Chem. Phys., 13(10), 5227–5241, doi:10.5194/acp-13-5227-2013, 2013.

Vestin, A., Rissler, J., Swietlicki, E., Frank, G. P. and Andreae, M. O.: Cloud-nucleating properties of the Amazonian

biomass burning aerosol: Cloud condensation nuclei measurements and modeling, J. Geophys. Res., 112(D14), D14201, doi:10.1029/2006JD008104, 2007.

Ward, D. S., Eidhammer, T., Cotton, W. R. and Kreidenweis, S. M.: The role of the particle size distribution in assessing aerosol composition effects on simulated droplet activation, Atmos. Chem. Phys., 10(2008), 5435–5447, doi:10.5194/acp-10-5435-2010, 2010.

Wex, H., McFiggans, G., Henning, S. and Stratmann, F.: Influence of the external mixing state of atmospheric aerosol on derived CCN number concentrations, Geophys. Res. Lett., 37(10), n/a-n/a, doi:10.1029/2010GL043337, 2010.

Wolfram Research, I.: Mathematica, Version 10.0, 2014.

Wu, L., Su, H. and Jiang, J. H.: Regional simulations of deep convection and biomass burning over South America: 1. Model evaluations using multiple satellite data sets, J. Geophys. Res., 116(D17), D17208, doi:10.1029/2011JD016105, 2011.

Table 1. Parameters for the Aitken and accumulation log-normal number size distribution for the defined case studies.

	N_m (cm^{-3})	d_m (nm)	σ_m
Case MP$_{5,1}$			
Aitken	5000	95	1.60
Accumulation	1000	180	1.50
Case MP$_{1,5}$			
Aitken	1000	95	1.60
Accumulation	5000	180	1.50
Case HP$_{5,5}$			
Aitken	5000	95	1.60
Accumulation	5000	180	1.50

Table 2. Number fractions for the hygroscopic groups in the externally mixed populations *Ext1* and *Ext2*.

$\kappa_{p_{eff}} = \sum \kappa_{p_{hg}} f_{hg}$	*Ext1*		*Ext2*	
	$f_{\kappa_p=0.04}$	$f_{\kappa_p=0.16}$	$f_{\kappa_p=0.04}$	$f_{\kappa_p=0.30}$
0.04	1.00	0.00	1.00	0.00
0.06	0.83	0.17	0.92	0.08
0.08	0.67	0.33	0.85	0.15
0.10	0.50	0.50	0.77	0.23
0.12	0.33	0.67	0.69	0.31
0.14	0.17	0.83	0.62	0.38
0.16	0.00	1.00	0.54	0.46
0.18	-	-	0.46	0.54
0.20	-	-	0.38	0.62
0.25	-	-	0.19	0.81
0.30	-	-	0.00	1.00

Table 3. Parameters for the simulations.

Parameter	Value / Range
Updraft velocity	0.1 - 10 m s^{-1}
Hygroscopicity parameter	
Int	0.02 - 0.60
Ext1	0.04 - 0.16
Ext2	0.04 - 0.30
Initial conditions	
Relative humidity	98 %
Temperature	293 K
Atmospheric pressure	900 hPa
Air parcel height	500 m
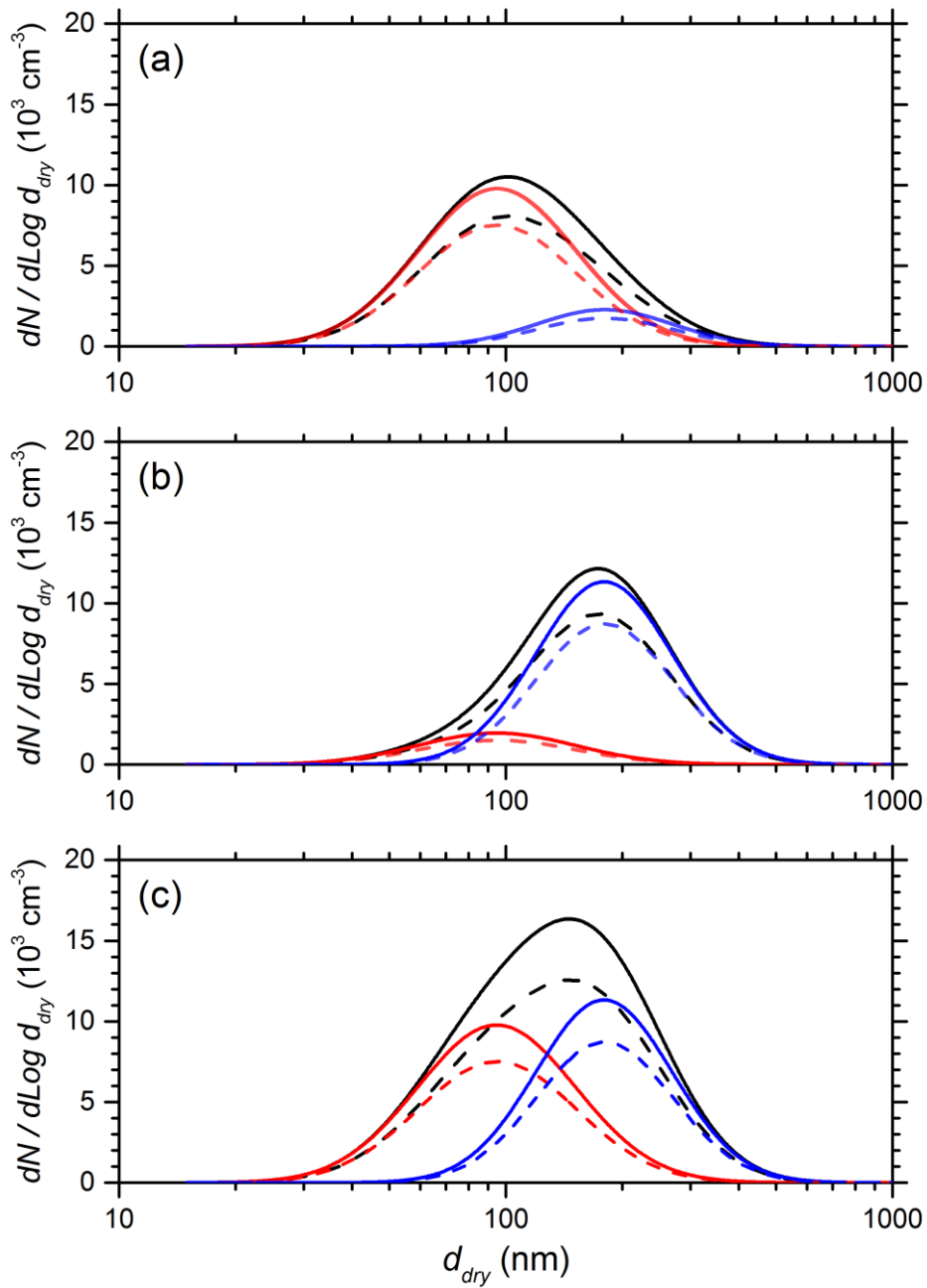
Figure 1. Schematic number size distributions for MP$_{5,1}$ (a), MP$_{1,5}$ (b) and HP$_{5,5}$ (c) case studies. Total population (black, solid), Aitken (red, solid) and accumulation (blue, solid) modes are indicated. Particles in hygroscopic group $\kappa_p = 0.04$ (dashed line, all colors) are also showed for a population average $\kappa_p = 0.10$.
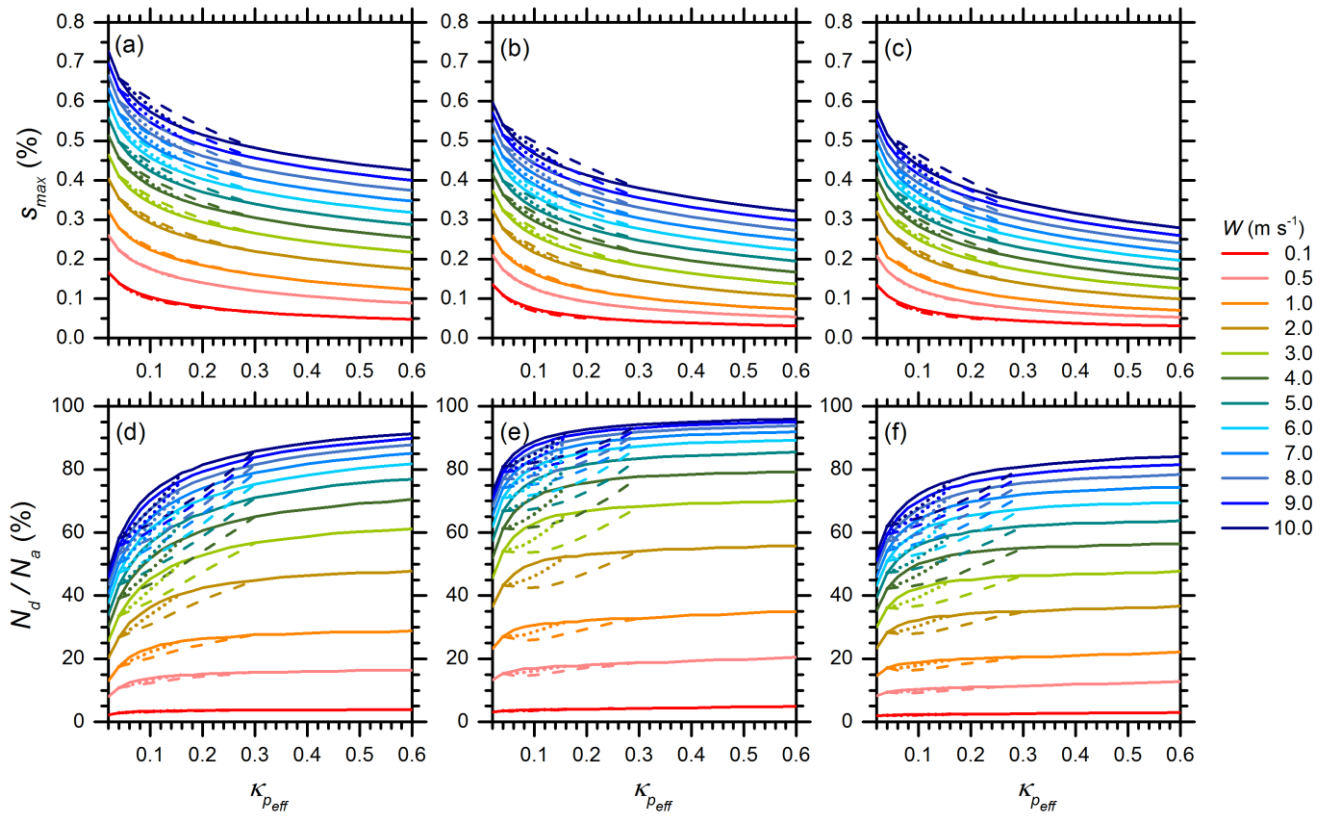
Figure 2. Maximum supersaturation reached (top) and fraction of particles activated (bottom) for the internal mixing (solid line) and external mixing cases *Ext1* (dotted line) and *Ext2* (dashed line). Plots on columns (a, d), (b, e) and (c, e) are for MP$_{5,1}$, MP$_{1,5}$ and HP$_{5,5}$ case studies, respectively. The color scale refers to the updraft velocities from 0.1 m s^{-1} and 10 m s^{-1}.
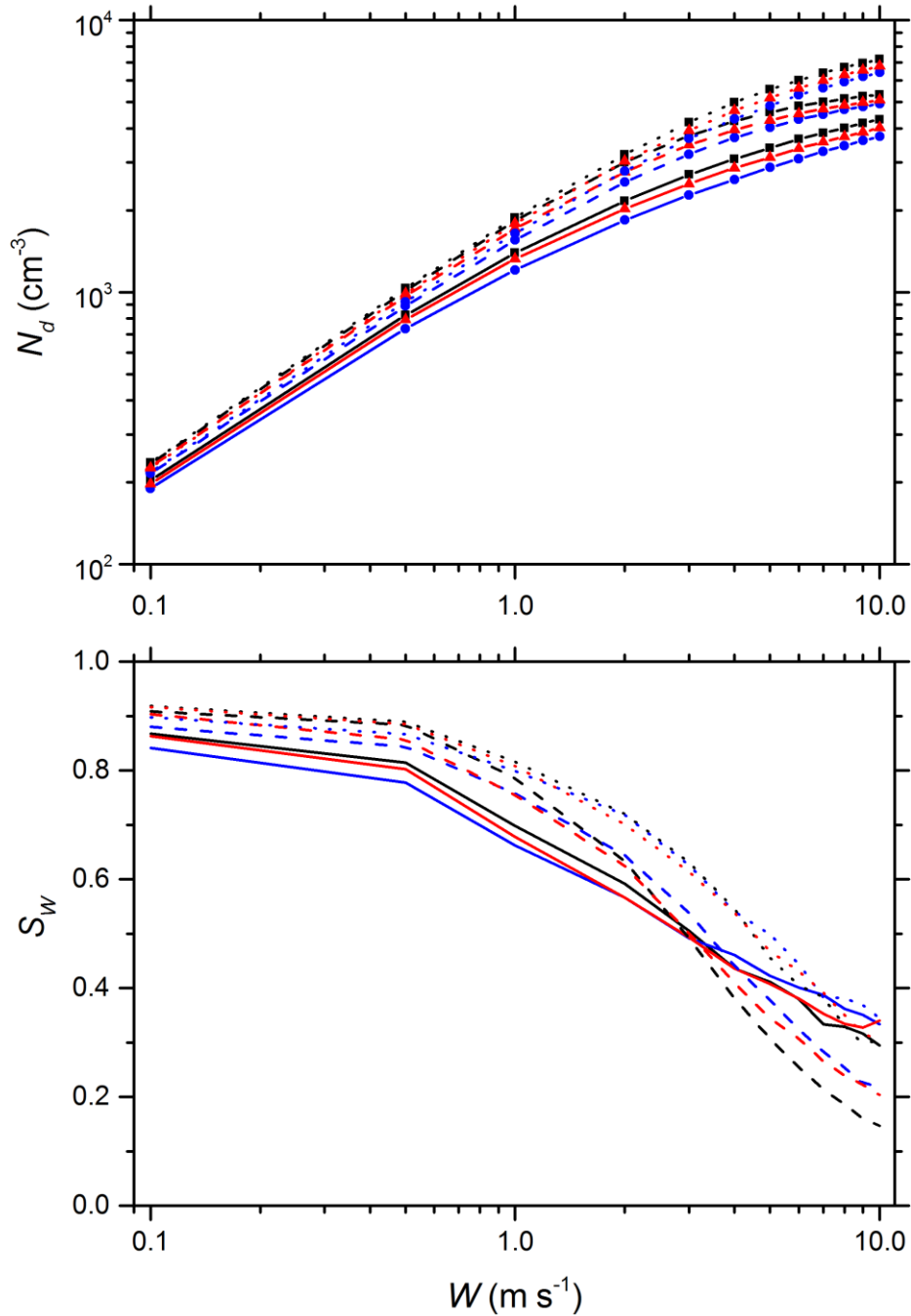
Figure 3. Number of particles activated (top) and sensitivity S_W of N_d to the updraft velocity W (bottom) for $\kappa_p = 0.10$, obtained for the MP$_{5,1}$ (solid line), MP$_{1,5}$ (dashed line) and HP$_{5,5}$ (dotted line) case studies. Results for internal mixed *Int* population and externally mixed populations *Ext1* and *Ext2* are in black, red and blue, respectively.
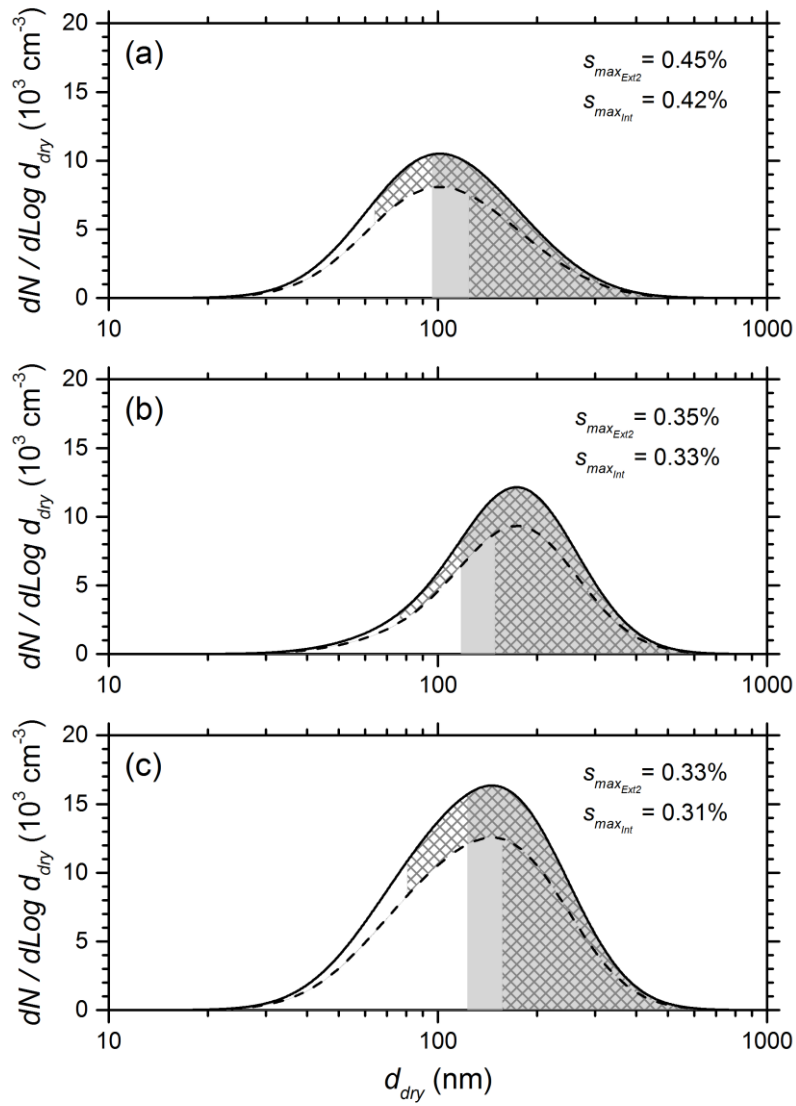
Figure 4. Schematic number size distribution of particles activated in *Ext2* (angled grid area) and *Int* (grey area) mixing states, for an average $\kappa_p = 0.1$ and W = 5 m s^{-1}, for (a) MP$_{5,1}$, (b) MP$_{1,5}$ and (c) HP$_{5,5}$ case studies. Total aerosol population (black, solid line), hygroscopic group $\kappa_p = 0.04$ (black, dashed line) and maximum supersaturation reached in the simulations for each mixing state are indicated.
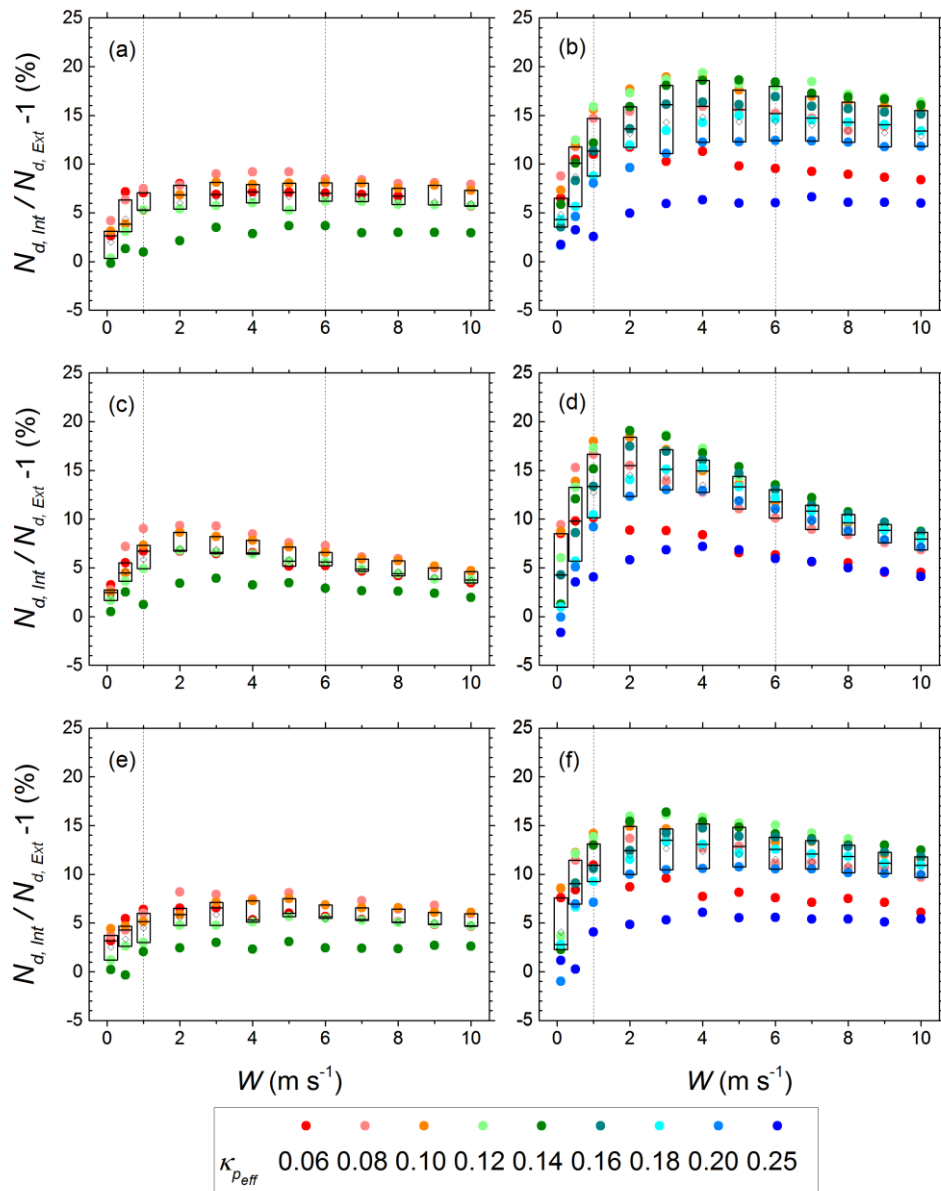
Figure 5. Overestimation of N_d when the aerosol is assumed to internally mixed, calculated as a function of the hygroscopicity (color scale) and the updraft velocity, for the external mixing *Ext 1* (left) and *Ext 2* (right). Plots on panels (a, b), (c, d) and (e, f) correspond to MP$_{5,1}$, MP$_{1,5}$ and HP$_{5,5}$ case studies, respectively. Box plots on top of data represent the spread for different hygroscopicity parameters. The box boundaries delimitate the interquartile range and mean values are indicated by diamond symbols. Dashed lines represent the approximate boundaries between CCN activation regimes.
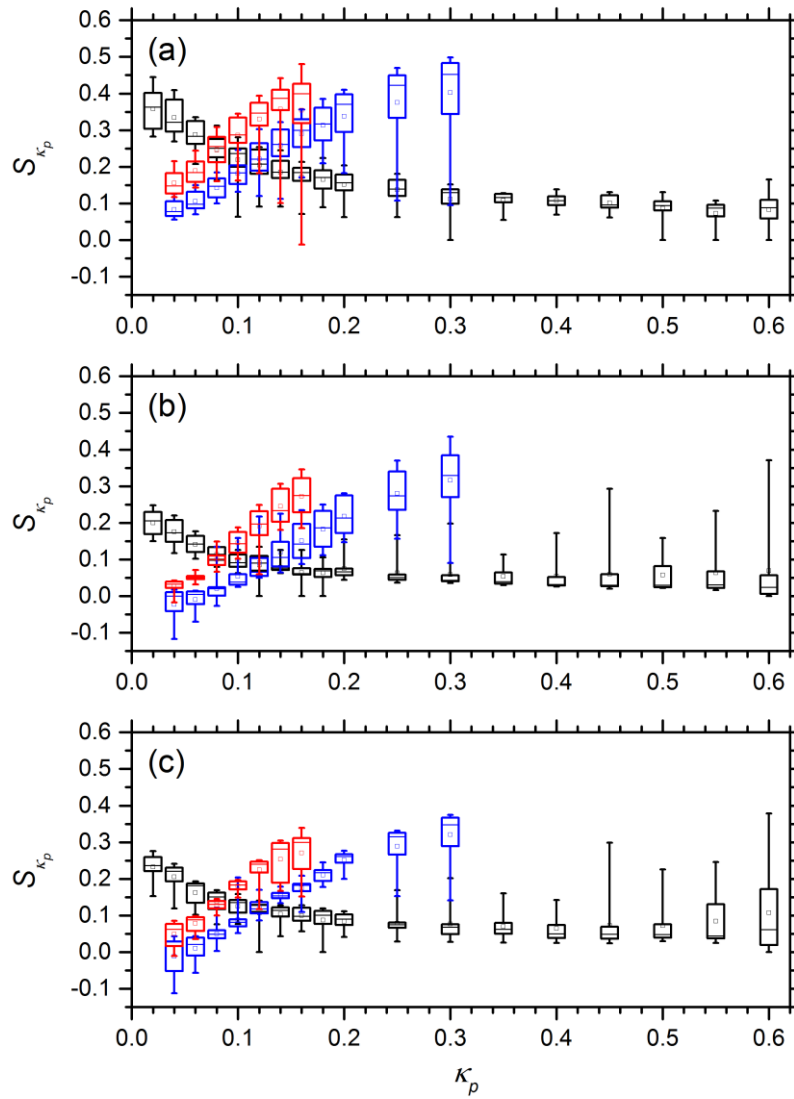
Figure 6. Box-whisker plots of the sensitivity S_{κ_p} of N_d to the hygroscopicity parameter κ_p, showing spread of results for updraft velocities between 0.1 m s^{-1} and 10 m s^{-1}, for (a) MP$_{5,1}$, (b) MP$_{1,5}$ and (c) HP$_{5,5}$ case studies. Box bounds show the interquartile range, the mean value is indicated by a small square and whiskers delimitate minimum and maximum values. Results for the internally mixed *Int* and externally mixed populations *Ext1* and *Ext2* are plotted in black, red and blue, respectively.
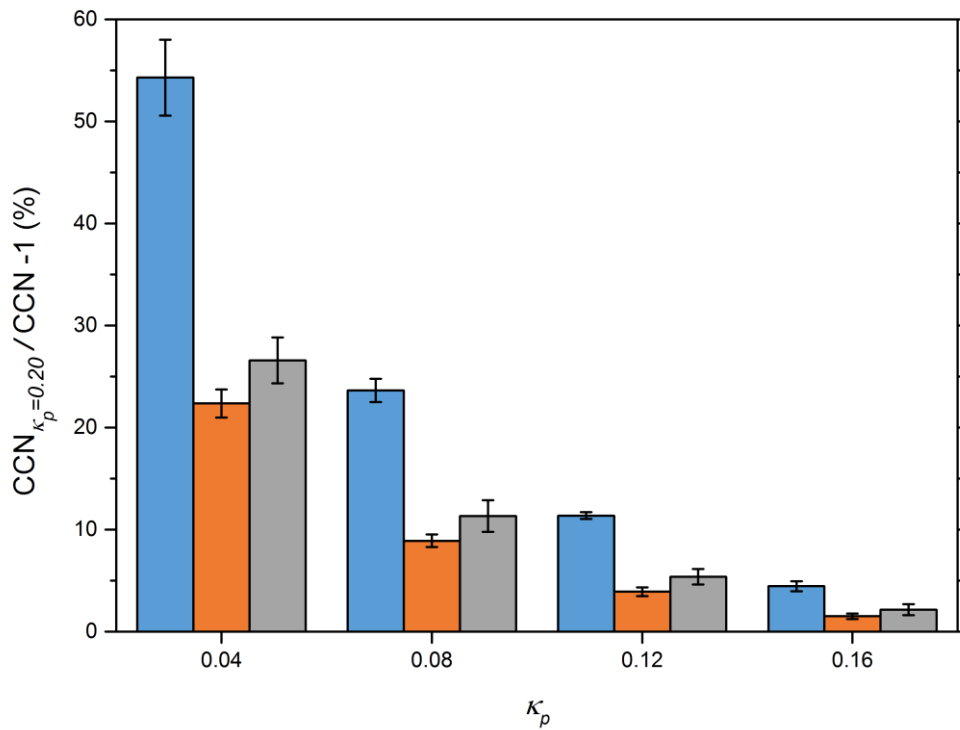
Figure 7. Overestimation of N_d (mean ± standard deviation over the updraft velocities in the updraft- and aerosol sensitive regime) when $\kappa_p = 0.20$ is assumed, as a function of the population κ_p. Results correspond to MP$_{5,1}$ (blue), MP$_{1,5}$ (orange) and HP$_{5,5}$ (grey) case studies for an internally mixed population.
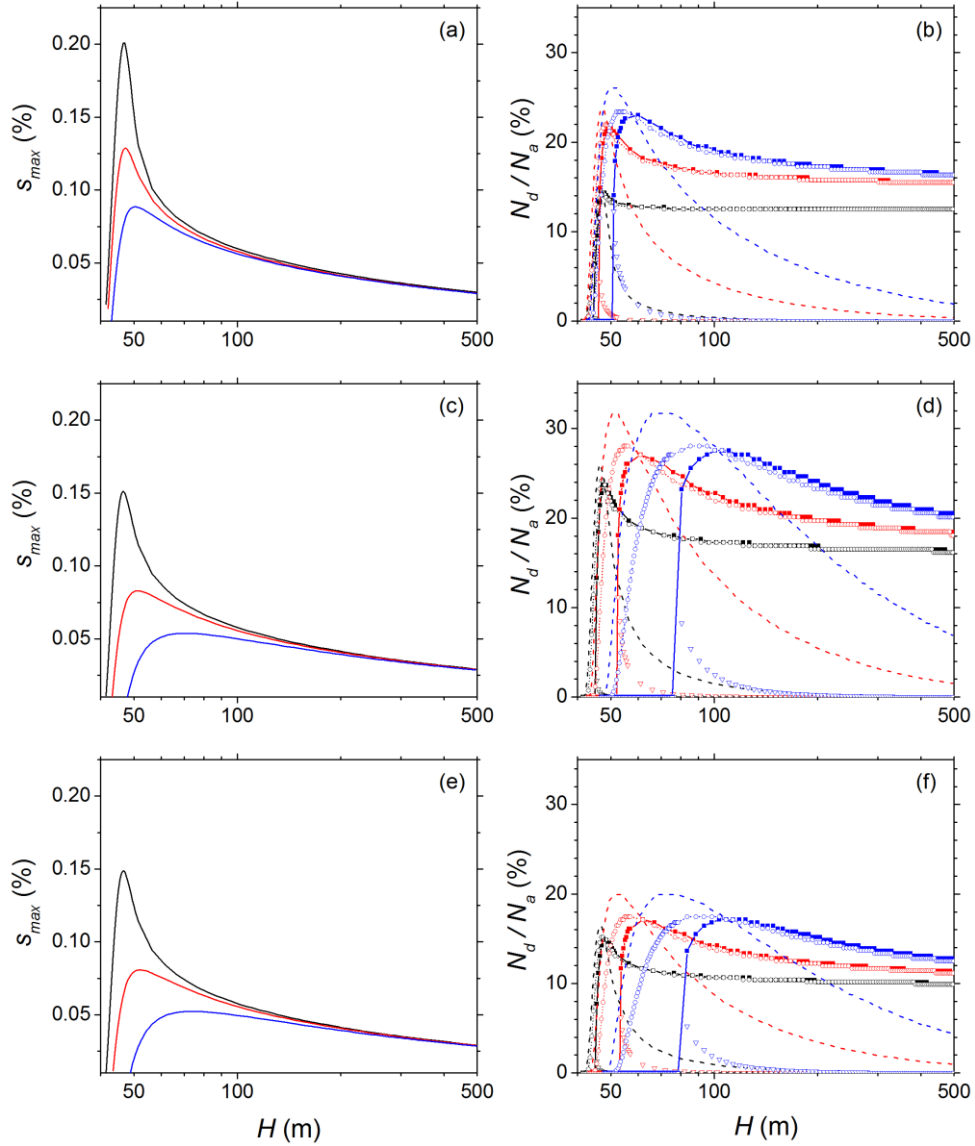
Figure 8. Supersaturation (left) and aerosol activated fraction (right) as a function of cloud height for an internally mixed population with $\kappa_p = 0.06$ (black), $\kappa_p = 0.25$ (red) and $\kappa_p = 0.60$ (blue), and $W = 0.5$ m s^{-1}. The cloud droplet concentration was estimated either as $N_{d,eq}$ (dashed line), N_{d,neq_simp} (solid line, open circles) or $N_{d,neq}$ (solid line, close squares). The fraction
5   **of the population not strictly activated in $N_{d,neq}$ is indicated (open down triangles). Plots on panels (a, b), (c, d) and (e, f) correspond to MP$_{5,1}$, MP$_{1,5}$ and HP$_{5,5}$ case studies, respectively.**
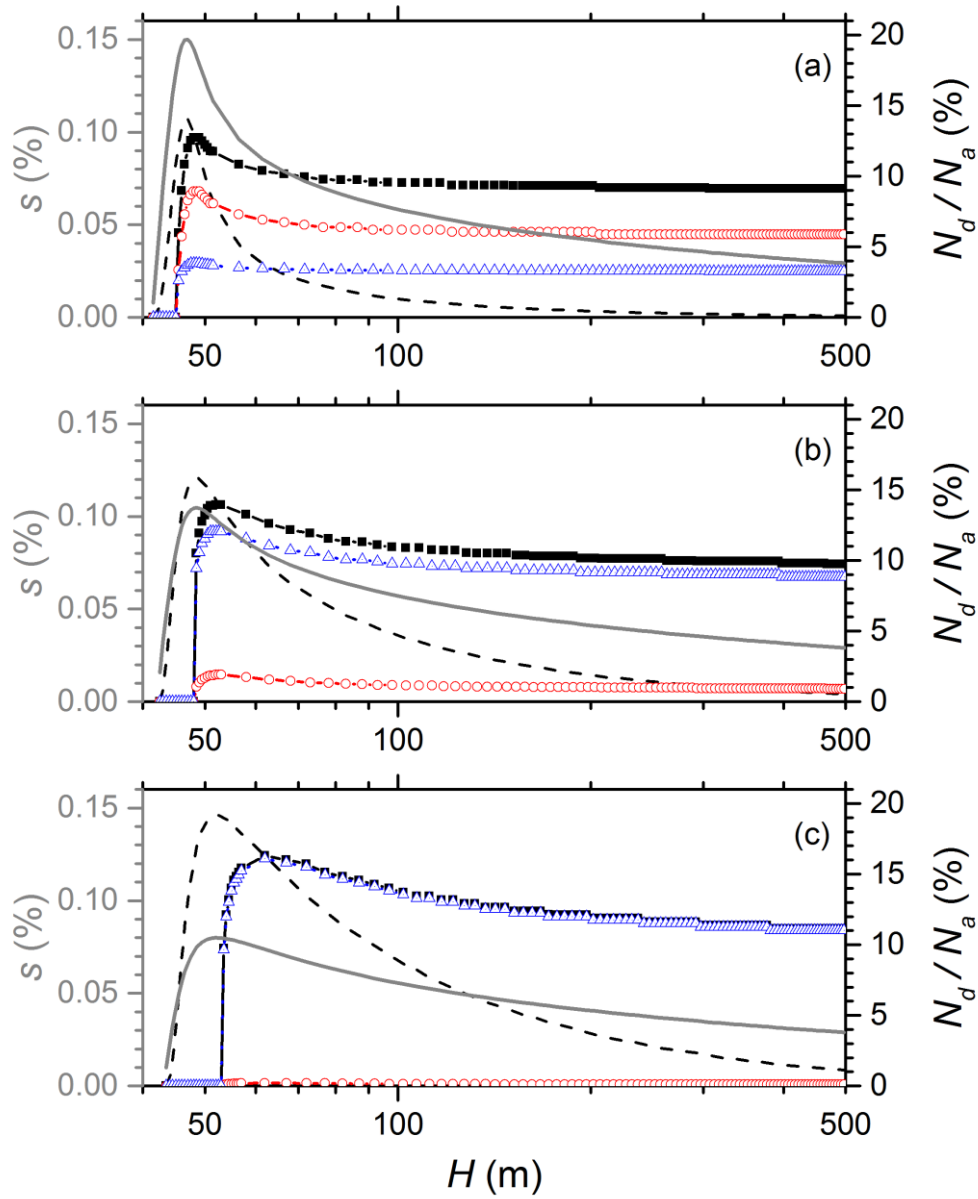
Figure 9. Supersaturation (left axis, grey) and aerosol activated fraction during the simulation (right axis) for the *Ext2* population and the HP$_{5,5}$ case study, for W = 0.5 m s^{-1} and $\kappa_{p_{eff}} = 0.06$ (a), $\kappa_{p_{eff}} = 0.14$ (b) and $\kappa_{p_{eff}} = 0.25$ (c). The cloud droplet concentration was estimated as $N_{d,eq}$ (dashed line), and $N_{d,neq}$ for the population (black solid line, close squares) and hygroscopic groups with $\kappa_p = 0.04$ (red dashed line, open circles) and $\kappa_p = 0.30$ (blue dotted line, open up triangles).
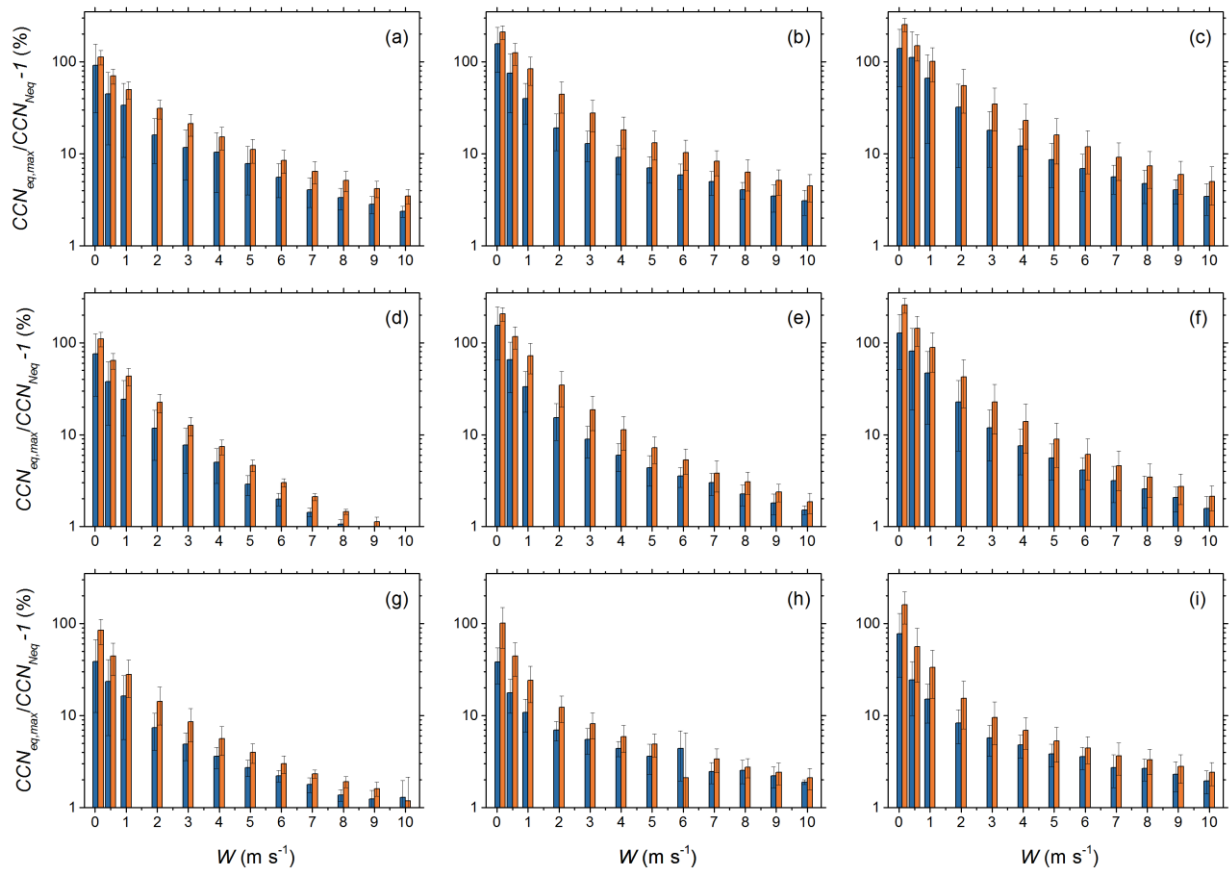
Figure 10. Overestimation of N_d when the population is estimated assuming equilibrium at the time of maximum supersaturation, $\max(N_{d,eq})$, compared with $N_{d,neq}$ at the time of maximum supersaturation (blue) and at the end of the simulation (orange), for the range of updraft velocities. Values correspond to the MP$_{5,1}$ (a, b and c panels), MP$_{1,5}$ (d, e and f panels) and HP$_{5,5}$ (g, h and i panels) case studies. The mixture of the aerosol population was either internal (left panels), or external as in *Ext1* (middle panels) and *Ext2* (right panels).